



# Receptor and Ionic Mechanism of Histamine on Mouse Dorsolateral Striatal Neurons

Jian-Ya Peng<sup>1</sup> · Kang-Li Shen<sup>1</sup> · Xiu-Juan Fan<sup>1</sup> · Zeng-Xin Qi<sup>2,3,4</sup> · Hui-Wei Huang<sup>1</sup> · Jian-Lan Jiang<sup>1</sup> · Jian-Hua Lu<sup>1</sup> · Xiao-Qin Wang<sup>1</sup> · Xiao-Xia Fang<sup>1</sup> · Wang-Rui Yuan<sup>1</sup> · Qiao-Xuan Deng<sup>1</sup> · Shu Chen<sup>1</sup> · Liang Chen<sup>2,3,4,5</sup> · Qian-Xing Zhuang<sup>1</sup>

Received: 10 June 2022 / Accepted: 8 October 2022 / Published online: 17 October 2022  
© The Author(s), under exclusive licence to Springer Science+Business Media, LLC, part of Springer Nature 2022

## Abstract

The dorsolateral striatum (DLS) is the critical neural substrate that plays a role in motor control and motor learning. Our past study revealed a direct histaminergic projection from the tuberomammillary nucleus (TMN) of the hypothalamus to the rat striatum. However, the afferent of histaminergic fibers in the mouse DLS, the effect of histamine on DLS neurons, and the underlying receptor and ionic mechanisms remain unclear. Here, we demonstrated a direct histaminergic innervation from the TMN in the mouse DLS, and histamine excited both the direct-pathway spiny projection neurons (d-SPNs) and the indirect-pathway spiny projection neurons (i-SPNs) of DLS via activation of postsynaptic H1R and H2R, albeit activation of presynaptic H3R suppressed neuronal activity by inhibiting glutamatergic synaptic transmission on d-SPNs and i-SPNs in DLS. Moreover, sodium-calcium exchanger 3 (NCX3), potassium-leak channels linked to H1R, and hyperpolarization-activated cyclic nucleotide-gated channel 2 (HCN2) coupled to H2R co-mediated the excitatory effect induced by histamine on d-SPNs and i-SPNs in DLS. These results demonstrated the pre- and postsynaptic receptors and their downstream multiple ionic mechanisms underlying the inhibitory and excitatory effects of histamine on d-SPNs and i-SPNs in DLS, suggesting a potential modulatory effect of the central histaminergic system on the DLS as well as its related motor control and motor learning.

**Keywords** Histamine · Dorsolateral Striatum · H1R · H2R · H3R · Ionic Mechanisms

Jian-Ya Peng, Kang-Li Shen, Xiu-Juan Fan, and Zeng-Xin Qi contributed equally to this work.

✉ Liang Chen  
hschenliang@fudan.edu.cn

✉ Qian-Xing Zhuang  
qxzhuang@ntu.edu.cn

<sup>1</sup> Department of Physiology, School of Medicine, and Co-Innovation Center of Neuroregeneration, Nantong University, 19 Qixiu Road, Nantong 226001, Jiangsu, China

<sup>2</sup> Department of Neurosurgery, Huashan Hospital, Shanghai Medical College, Fudan University, Shanghai 200030, China

<sup>3</sup> National Center for Neurological Disorders, Shanghai 200030, China

<sup>4</sup> Shanghai Key Laboratory of Brain Function Restoration and Neural Regeneration, Shanghai 200030, China

<sup>5</sup> State Key Laboratory of Medical Neurobiology and MOE Frontiers Center for Brain Science, School of Basic Medical Sciences and Institutes of Brain Science, Fudan University, Shanghai 200030, China

## Abbreviations

DLS	Dorsolateral striatum
TMN	Tuberomammillary nucleus
d-SPNs	Direct-pathway spiny projection neurons
i-SPNs	Indirect-pathway spiny projection neurons
NCX3	Sodium-calcium exchanger 3
HCN2	Hyperpolarization-activated cyclic nucleotide-gated channel 2
H1R	Histamine H1 receptor
H2R	Histamine H2 receptor
H3R	Histamine H3 receptor
H4R	Histamine H4 receptor
AAV	Adeno-associated virus
EGFP	Enhanced green fluorescent protein
ACSF	Artificial cerebrospinal fluid
ELISA	Enzyme-linked immunosorbent assay
PD	Parkinson's disease

## Introduction

As a general modulator for the entire brain activity, the central histaminergic system, which originates from the tuberomammillary nucleus (TMN) of the hypothalamus, sends its fibers widely to almost the entire brain regions [1, 2]. The central histaminergic nervous system was originally believed to play an essential regulatory role in non-somatic functions, such as the sleep–wake cycle, endocrine balance, learning, and memory [3, 4]. However, an increasing number of studies have demonstrated that histamine also participates in somatic motor functions such as motor control and motor balance by affecting the activities of subcortical motor structures, including the basal ganglia [5, 6]. However, knowledge about the role of central histaminergic afferents in basal ganglia remains limited.

The dorsolateral striatum (DLS) is roughly homologous to the putamen in primates, it contains two types of projection neurons, the direct pathway spiny projection neurons (d-SPNs) and the indirect pathway spiny projection neurons (i-SPNs), which constitute the starting points of the direct (striatonigral) pathway and the indirect (striatonigral) pathway in the basal ganglia circuit, respectively [7, 8]. The DLS holds a critical position in motor functions, such as motor control and motor learning [9–11]. It receives glutamatergic afferents from the cortex (including the sensory, motor, and associational cortex) and thalamus, such as the intralaminar thalamic nuclei; this excitatory input is then regulated by local GABAergic interneurons and collateral inhibition of its adjacent DLS projection neurons [9, 12, 13]. The balance of excitatory and inhibitory transmission in the dorsal striatum is modulated by neuromodulators such as dopamine from substantia nigra pars compacta, serotonin from dorsal raphe, acetylcholine and neuropeptide-Y from local interneurons [14–16]. These neuromodulators are critical for regulating striatal circuits, and disruption of this signaling can result in movement disorders and neurological disorders such as motor deficits and cognitive impairments [10, 17, 18].

In addition to the abovementioned classical neuromodulators of striatal neurons, the impact of hypothalamic histaminergic modulation on striatal neurons has received increasing attention in recent years [5, 19, 20]. Importantly, we recently demonstrated histaminergic innervation in the striatum and histamine excited rat striatum neurons *in vitro* [5]. However, the histaminergic innervation in DLS and the receptor and ionic mechanisms underlying the effect of histamine on d-SPNs and i-SPNs of mouse DLS remain largely unclear. Therefore, in the present study, we employed brain stimulation, microdialysis, anterograde tracing, immunostaining, single-cell qPCR, whole-cell patch-clamp recording, and CRISPR/

Cas9 gene-editing techniques on D1-Cre, D2-Cre, and LSL-Cas9-tdTomato::D1/D2-Cre mice. We detected a direct histaminergic innervation in DLS from TMN, and histamine directly excited the d-SPNs and i-SPNs through activation of postsynaptic H1R and H2R and that the two histamine receptor subtypes were co-expressed and colocalized on the same d-SPNs or i-SPNs. Moreover, histamine inhibited the activity of d-SPNs and i-SPNs through the activation of presynaptic H3R. Furthermore, the potassium leak channels and sodium-calcium exchanger 3 (NCX3) linked to H1R and the hyperpolarization-activated cyclic nucleotide-gated channel 2 (HCN2) linked to H2R co-mediated the histamine-induced excitation on d-SPNs and i-SPNs in DLS.

## Materials and Methods

### Animals

Six to 8-week-old B6/JGpt-*Drd1*<sup>em1Cin(P2A-iCre)</sup>/Gpt (D1-Cre), B6/JGpt-*Drd2*<sup>em1Cin(P2A-iCre)</sup>/Gpt (D2-Cre), and B6/JGpt-Rosa26<sup>tm1Cin(CAG-LSL-Cas9-tdTomato)</sup>/Gpt mice (LSL-Cas9-tdTomato) mice were obtained from GemPharmatech Co., Ltd (Jiangsu, China) and wild-type (WT) C57BL/6 J mice were from Experimental Animal Center of Nantong University (Nantong, China), all the mice were housed in SPF condition of Experimental Animal Center of Nantong University. Mice of either sex were individually housed under controlled environmental conditions (22 ± 2 °C; 60 ± 5% humidity; and a 12-h light/dark cycle with lights on at 8:00 am; daily). The animals had free access to standard laboratory chow and water. Animal maintenance and experiments were under the US National Institutes of Health Guide for the Care and Use of Laboratory Animals (NIH Publication 85–23, revised 2011), and they were approved by the Institutional Animal Care and Use Committee of Nantong University. All efforts were made to minimize the number of animals used and their suffering.

### *In vivo* Microdialysis Sampling, TMN Stimulation, and Assay for Histamine

The microdialysis methods have been described previously [21]. Briefly, after anesthetized by isoflurane (4% for induction, 1.5% for maintenance), adult mice weighing 20–25 g were placed in a stereotaxic frame (1404, David Kopf Instruments). Guide cannulas were stereotaxically implanted into the brain to allow the positioning of a CMA/7 microdialysis probe (CMA/Microdialysis, Stockholm, Sweden) with 1 mm membrane length into three sites of the right DLS (AP1: 1.18 mm, ML1: ± 1.75 mm, DV1: – 2.0 mm) (AP2: 0.62 mm, ML2: ± 2.0 mm, DV2: – 2.0 mm) (AP3: 0.02 mm,

ML3:  $\pm 2.38$  mm, DV3:  $-2.0$  mm) [22]. At the same time, the mice were implanted with stimulation electrodes (stainless steel, Teflon coated, 100  $\mu\text{m}$  in diameter) aimed at the right TMN (AP:  $-2.3$  mm, ML:  $\pm 1.15$  mm, DV:  $-5.25$  mm). Probe and electrode placement was verified histologically at the end of the experiment. Mice were allowed to recover in individual cages for at least 3 days. Then, in freely moving mice, a microdialysis probe was inserted through the guide, and the probe was perfused with ACSF (composition in mM: 125 NaCl, 2.5 KCl, 1.25  $\text{NaH}_2\text{PO}_4$ , 1.3  $\text{MgSO}_4$ , 26  $\text{NaHCO}_3$ , 2.5  $\text{CaCl}_2$ , and 10 D-glucose) for 240 min at a flow rate of 10  $\mu\text{l}/\text{min}$  before sample collection. Microdialysis samples were collected in 30-min intervals using a MAB 85 fraction collector (CMA/Microdialysis) through the microdialysis probe at 0.5  $\mu\text{l}/\text{min}$  using a CMA 402 syringe pump (CMA/Microdialysis) during TMN stimulation (1 min train of 0.1 ms pulses of 100  $\mu\text{A}$  and 100 Hz every 5 min for 30 min), rectangular electrical stimulation was applied using a Master-8 stimulator (AMPI, Jerusalem, Israel) [23, 24]. During the stimulation in freely moving mice, the stimulation intensity was gradually increased until behavioral abnormalities, such as evidence of stress characterized by vocalization, excessive locomotor activity, escape behavior, or biting, and then 30% of this intensity was chosen as the current for stimulation [25]. The first two 30-min samples were discarded, and the subsequent samples were collected for analysis of basal extracellular levels of histamine. Histamine content was measured by a commercial enzyme-linked immunosorbent assay (ELISA) kit (Cayman Chemical, Ann Arbor, MI) according to the manufacturer's protocol. Histamine content was expressed as picograms per milliliter of microdialysis samples.

## Stereotactic Surgeries and Injections

Under deep anesthesia induced by isoflurane (4% for induction, 1.5% for maintenance), mice weighing 20–25 g were placed into a stereotaxic frame (1404, David Kopf Instruments, Tujunga, CA) for brain surgery under aseptic conditions, and a 1–2 cm incision was made in the scalp to expose the skull. A small hole was drilled in the skull, and the dura was gently broken to allow uninterrupted passage of the micropipette.

For anterograde tracer biotinylated dextran amine (BDA; Ref: D-1956 from Thermo Fisher Scientific, Waltham, MA) injection, 10% BDA in 0.01 M phosphate-buffered saline (PBS; pH 7.4) was injected into TMN (AP:  $-2.70$  mm, ML: 1.10 mm, DV: 5.05 mm) according to the mouse brain atlas [22], injections were made under 5  $\mu\text{A}$  positive alternating current (7 s on/7 s off) for 40 min, followed by a 10 min rest period. Once completed, the micropipette was left in place for 5 min before removal. During micropipette withdrawal,

the current was reversed to minimize tracer leakage through the injection tract.

For adeno-associated virus (AAV) injection, the viral solution was injected at three sites of the DLS (AP1: 1.18 mm, ML1:  $\pm 1.75$  mm, DV1:  $-2.0$  mm) (AP2: 0.62 mm, ML2:  $\pm 2.0$  mm, DV2:  $-2.0$  mm) (AP3: 0.02 mm, ML3:  $\pm 2.38$  mm, DV3:  $-2.0$  mm) according to the mouse brain atlas [22] in D1 or D2-Cre mice. The injection volume of AAV9-hSyn-DIO-EGFP (viral titers were  $3.12 \times 10^{13}$  viral genomes per milliliter, Obio Technology Company, Shanghai, China) was 0.15  $\mu\text{l}/\text{site}$ . The injection volume of AAV9-CMV-*Ncx3* sgRNA-EGFP targeting 5'-GAGCAG AGGCTGGTACTCGGGG-3', 5'-CCTTGGGGACAA GATTGCCAGGG-3', and 5'-TCGGGGGATGTGCC AGTGCAGG-3' (viral titers were  $1.0 \times 10^{13}$  viral genomes per milliliter, PackGene, Guangzhou, China) or AAV9-CMV-neg-EGFP (control virus, viral titers were  $1.32 \times 10^{13}$  viral genomes per milliliter, PackGene) was 0.2  $\mu\text{l}/\text{site}$ . The injection volume of AAV9-CMV-*Hcn2* sgRNA-EGFP targeting 5'-GGGCGGCCGGGCGATAGTCCGGG-3', 5'-TCC GGGCACGACCCCTGCGCCGG-3', and 5'-CGGGCA CGACCCCTGCGCCGGGG-3' (viral titers were  $4.2 \times 10^{12}$  viral genomes per milliliter, Genechem, Shanghai, China) or AAV9-CMV-neg-EGFP (control virus, viral titers were  $6.5 \times 10^{12}$  viral genomes per milliliter, Genechem) was 0.3  $\mu\text{l}/\text{site}$ .

All the AAV vectors and BDA were microinjected with Hamilton syringe(s) (2.5  $\mu\text{l}$ , 7632–01) controlled by a syringe pump (KDS100, KD Scientific, MA) at a rate of 20 nL/min. Once completed, the micropipette was left in place for 5 min before removal. Mice that received successful tracer or virus injections were allowed to survive for three weeks before the terminal experiments were conducted.

## Immunohistochemistry and Imaging

Mice (weighing 20–25 g) were deeply anesthetized with isoflurane (4% for induction, 1.5% for maintenance) and perfused transcardially with 50 ml normal saline, followed by 100–150 ml 4% paraformaldehyde in 0.1 M phosphate buffer. Subsequently, the brain was removed, trimmed, and postfixed in the same fixative for 12 h at 4 °C, the brain was successively cryoprotected with 20% and 30% sucrose for 24 h. Frozen coronal sections containing the DLS were obtained using a freezing microtome (CM1850, Leica, Heidelberg, Germany) and mounted on gelatin-coated slides. The slices were rinsed with PBS containing 0.1% Triton X-100 and then incubated in 10% normal bovine serum in PBS containing 0.1% Triton X-100 for 30 min.

Sections were incubated overnight at 4 °C with primary antibodies: mouse anti-GAD67 (1:500, MilliporeSigma, catalog MAB5406, RRID:AB\_2278725), rabbit anti-H1R polyclonal antibody (1:400, Alomone Labs, Jerusalem,

Israel; catalog #AHR-001, RRID: AB\_2039915), goat anti-H2R polyclonal antibody (1:500, Everest Biotech; catalog EB06905, RRID:AB\_2121375), rabbit anti-HCN1 (1:300, Alomone Labs; catalog APC-056, RRID:AB\_2039900), rabbit anti-HCN2 (1:100, Alomone Labs; catalog APC-030, RRID:AB\_2313726), rabbit anti-HCN3 (1:100, Alomone Labs; catalog APC-057, RRID:AB\_2039904), and rabbit anti-HCN4 (1:200, Alomone Labs; catalog APC-052, RRID:AB\_2039906). These primary antibodies were validated for species and application (1DegreeBio and Antibody Registry). After a complete wash in PBS, the sections for double or triple immunostaining were incubated in the related Alexa Fluor 488-, Alexa Fluor 594-, Alexa Fluor 350-, and/or Alexa 594-conjugated streptavidin secondary antibodies (1:2000, Thermo Fisher Scientific) for 2 h at room temperature in the dark. The slides were washed and mounted in Fluoromount-G mounting medium (Southern Biotech, Cambridge, UK). Incubation solution replacing the primary antiserum with control immunoglobulins and, or omitting the primary antiserum was used as negative controls. All micrographs were taken with an inverted laser scanning confocal microscopy (model SP2 TCS; Leica, Heidelberg, Germany), equipped with Plan-Apochromat  $\times 40/0.9$  NA oil,  $\times 20/0.75$  NA dry, and  $\times 10/0.4$  NA dry objective lenses. Digital images from the microscope were recorded with Leica Application Suite imaging and analysis software (Leica), and image processing was done with Photoshop (Adobe Systems Inc., San Jose, CA).

The number of the labeled DLS neurons was quantified by numerical density, estimated by counting the number of neurons within 3D optical dissectors that were systematically spaced at random throughout the selected brain areas. Ten optical dissectors sized  $80 \times 80 \times 30 \mu\text{m}$  were randomly sampled, and the number of positive cells in each dissector was quantified. The density of cells was estimated using the following formula:  $Nv = Q/v$  (dis), where “ $Q$ ” is the average number of cells counted per dissector, and “ $v$  (dis)” is the volume of the dissector:  $v$  (dis) =  $a$  [frame]  $\times h$ , where “ $a$ ” is an area of the frame and “ $h$ ” is dissector height. Data were represented as the number of cells per cubic millimeter.

### Patch Clamp Recordings In vitro

To assess the receptor and ionic mechanisms of histamine on DLS neurons, whole-cell patch-clamp recordings were performed as previously described [5]. After decapitation under deeply anesthetized with isoflurane (4%), the slices containing DLS from adult mice of either sex were identified according to the mouse brain atlas [22], and incubated in oxygenated artificial cerebrospinal fluid (ACSF, composition in mM: 125 NaCl, 2.5 KCl, 1.25  $\text{NaH}_2\text{PO}_4$ , 1.3  $\text{MgSO}_4$ , 26  $\text{NaHCO}_3$ , 2.5  $\text{CaCl}_2$ , and 10 D-glucose) at  $35 \pm 0.5$  °C for at least 1 h. And the  $\text{Tris}^+$  ACSF for  $\text{Na}^+$  replacement

experiment by using  $\text{Tris}^+$  to inactivate NCXs was as follows (composition in mM): 125  $\text{Tris-Cl}$ , 2.5 KCl, 1.25  $\text{NaH}_2\text{PO}_4$ , 1.3  $\text{MgSO}_4$ , 26  $\text{NaHCO}_3$ , 2.5  $\text{CaCl}_2$ , and 10 D-glucose. Sections were then kept at room temperature for approximately 30 min before recording. Finally, during recording, the slices were transferred into the submerged chamber and continuously perfused with oxygenated ACSF at a rate of 2 ml/min maintained at  $32 \pm 0.5$  °C.

Whole-cell patch-clamp recordings were performed with borosilicate glass pipettes (4–6 M $\Omega$ ) filled with an internal solution (composition in mM): 135 KMeSO<sub>4</sub>, 10 Na<sub>2</sub>-phosphocreatine, 5 KCl, 0.5  $\text{CaCl}_2$ , 5 HEPES, 5 EGTA, 2  $\text{Mg}_2\text{ATP}$ , 0.5 Na<sub>3</sub>GTP, adjusted to pH 7.25 with KOH. The internal solution for spontaneous excitatory postsynaptic currents (sEPSCs) recordings consisted of the following (in mM): 125 CsMeSO<sub>3</sub>, 10 Na<sub>2</sub>-phosphocreatine, 5 tetraethylammonium chloride, 1 QX-314 Cl, 5 HEPES, 0.25 EGTA, 2  $\text{Mg}_2\text{ATP}$ , 0.5 Na<sub>3</sub>GTP, adjusted to pH 7.25 with CsOH. The internal solution for spontaneous inhibitory postsynaptic currents (sIPSCs) recordings consisted of the following high  $\text{Cl}^-$  solution (in mM): 110 CsCl, 10 NaCl, 5  $\text{MgCl}_2$ , 0.6 EGTA, 40 HEPES, 2  $\text{Mg}_2\text{ATP}$ , 5 QX314, 0.2 Na<sub>3</sub>GTP, adjust to pH 7.2 with CsOH.

Both d-SPNs and i-SPNs in DLS were visualized with an Olympus BX51WI microscope (Tokyo, Japan) equipped with infrared differential interference contrast and fluorescence mode. All images were captured with a CoolSNAP cf Photometrics camera (Roper Scientific, Rochester, NY), displayed in a laboratory computer. Patch-clamp recordings were acquired with an Axopatch-700B amplifier (Axon Instruments, Sunnyvale, CA), and the signals were fed into the computer through a Digidata-1440 interface (Axon Instruments) for data capture and analysis (pClamp 10.0, Axon Instruments). Recordings of whole-cell currents were lowpass filtered at 2 kHz and digitized at 10 kHz, and recordings of membrane potentials were lowpass filtered at 5 kHz and digitized at 20 kHz. Neurons were held at a membrane potential of  $-70$  mV and characterized by injection of rectangular voltage pulse (5 mV, 50 ms) to monitor the whole-cell membrane capacitance, series resistance, and membrane resistance. Neurons were excluded from the study if the series resistance was not stable or exceeded 30 M $\Omega$ . If the seal resistance changed more than 30% of the original, the neuron was abandoned and excluded from further analysis.

We bathed the slices with histamine (0.03–30  $\mu\text{M}$ , Tocris, Ellisville, MO) to stimulate the recorded DLS neurons. Before bath application, the whole-cell current or spontaneous firing rate of the recorded neuron was observed for at least 20 min to assure stability. Then, histamine was added to the ACSF to stimulate the recorded neuron for a test period of 1 min. After each stimulation, cells were given at least 20 min for recovery and prevention of desensitization.



TTX (0.3  $\mu\text{M}$ , Alomone Labs) was used to diminish network activity. AMPA receptor antagonist NBQX (10  $\mu\text{M}$ , Tocris), NMDA receptor antagonist D-AP5 (20  $\mu\text{M}$ , Tocris) were used to block the glutamatergic synaptic transmission, GABA<sub>A</sub> receptor antagonist SR95531 (10  $\mu\text{M}$ , Tocris) were used to block the GABAergic synaptic transmission.

Selective agonists for histamine receptor subtypes, 2-PyEA (100  $\mu\text{M}$ , Tocris), dimaprit (30  $\mu\text{M}$ , Tocris), VUF8430 (30  $\mu\text{M}$ , Tocris), and (*R*)-(-)- $\alpha$ -Methylhistamine (RAMH, 10  $\mu\text{M}$ , Tocris), as well as selective antagonists, mepyramine (0.3–1  $\mu\text{M}$ , Tocris), ranitidine (0.3–1  $\mu\text{M}$ , Tocris), JNJ7777120 (10  $\mu\text{M}$ , Tocris), Iodophenpropit (1  $\mu\text{M}$ , Tocris), SEA0400 (10  $\mu\text{M}$ , Tocris), ZD7288 (10  $\mu\text{M}$ , Tocris), 4-aminopyridine (4-AP, 10  $\mu\text{M}$ , Tocris), and H89 (10  $\mu\text{M}$ , Tocris) were applied to examine the underlying postsynaptic receptor mechanism. The receptor antagonists or ion channel blockers were given for at least 15 min before we observed their effects.

The mean concentrations of histamine for the half-maximal activation (EC<sub>50</sub>) for d-SPNs and i-SPNs were established by nonlinear regression, limiting the fitted peak to the highest experimental value (GraphPad Prism, 6.0 for Windows, GraphPad Software, San Diego, CA). To test the firing properties induced by histaminergic drugs, under the current-clamp mode, a series of positive current injections with a duration of 0.5 s and an interval of 5 s (ranging from 0 to 200 pA in 10-pA steps) was used to stably induce 2–7 action potentials [26]. During stimulation intervals, the membrane potential was maintained at about –70 mV by injecting hyperpolarizing/depolarizing currents to counteract possible H1R- H2R-dependent depolarization and H3R-dependent hyperpolarization [27]. To characterize the 2-PyEA-induced whole-cell current, under the voltage-clamp mode, current–voltage plots (*I*-*V* curves) were obtained before and during 2-PyEA application using a slow ramp command ( $dV/dt = -10$  mV/s, ranging from –70 to –130 mV) to allow for the attainment of steady-state conditions. In addition, to examine the effect of dimaprit on the HCN channel current (*I<sub>h</sub>*), *I*-*V* curves were obtained before and during dimaprit application using a series of 1 s hyperpolarizing voltage steps (ranging from –70 to –130 mV in –10 mV steps) [6]. *I<sub>h</sub>* was determined by subtracting instantaneous current from the maximum current at each hyperpolarizing voltage step, and *I<sub>h</sub>* current density was estimated as the amplitude of *I<sub>h</sub>* measured at various potentials (*V*) divided by the membrane capacitance (*C<sub>m</sub>*): *I<sub>h</sub>* current density = *I<sub>h</sub>*/*C<sub>m</sub>* [21].

### Single-Cell qPCR

Single-cell qPCR was performed as previously described [5]; briefly, following the patch-clamp recording experiment, the cytoplasm of the identified d-SPNs or i-SPNs

was pipetted into a recording pipette filled with 3–5  $\mu\text{L}$  of RNase-free solution and drained into a 0.2 ml PCR tube containing Single Cell Lysis/Dnase I solution using the Single Cell-to-CT Kit (Life Technologies). Reverse transcription and cDNA pre-amplification were performed on a thermal cycler (Applied Biosystems, Foster City, CA) according to the kit protocol. qPCR was performed using the TaqMan Gene Expression Assay system. The TaqMan assay probes were designed and purchased from Life Technologies as follows: Mm01183516\_m1 for *Hrh1*, Mm01337447\_m1 for *Hrh2*, Mm00468832\_m1 for *Hcn1*, Mm00468538\_m1 for *Hcn2*, Mm01212852\_m1 for *Hcn3*, Mm01176086\_m1 for *Hcn4*, Mm01232254\_m1 for *Ncx1*, Mm00455836\_m1 for *Ncx2*, Mm01309304\_m1 for *Ncx3*, and Mm99999915\_g1 for *gapdh*. Conditions for the cycles followed the manufacturer's protocol for TaqMan assays. The data were collected using the instrument's software (Rotor-Gene software, version 6.0, Corbett Research, Sydney, Australia), and relative quantification was performed using the comparative threshold (Ct) method after determining the Ct values for reference gene (*gapdh*) and target genes in each sample set according to the  $2^{-\Delta\Delta\text{Ct}}$  method. Changes in mRNA expression levels were calculated after normalization to *gapdh*.

### Statistical Analysis

All data were analyzed with SPSS 17.0 (SPSS, Chicago, IL) and presented as mean  $\pm$  SEM. Two-tailed paired or unpaired *t*-test was used for tests in two groups, one-way or two-way analysis of variance (ANOVA), one-way or two-way repeated measures analysis of variance (RM-ANOVA) followed by Student–Newman–Keuls (SNK) post hoc testing was used for tests in three or more groups. A threshold of  $P < 0.05$  was accepted as statistically different. Significance levels of the data were denoted as \* $P < 0.05$ , \*\* $P < 0.01$ , and \*\*\* $P < 0.001$ .  $P > 0.05$  was considered nonsignificant and denoted as ns.

## Results

### A Direct Histaminergic Projection from TMN to DLS

To determine the direct histaminergic afferent to the DLS, we measured the histamine concentration in DLS by microdialysis sampling during TMN stimulation and subsequent ELISA assay. When compared with control, the histamine concentration was elevated significantly during TMN stimulation (Fig. 1a–c); it was  $103.1 \pm 6.9$  pg/mL in pre-stimulation and  $220.5 \pm 9.3$  pg/mL during stimulation in DLS ( $n = 8$ ,  $P < 0.001$ ). Furthermore, the histaminergic fibers were found to be adjacent to the large GAD67-immunoreactive GABAergic neurons of the DLS (Fig. 1d, e). As most histaminergic

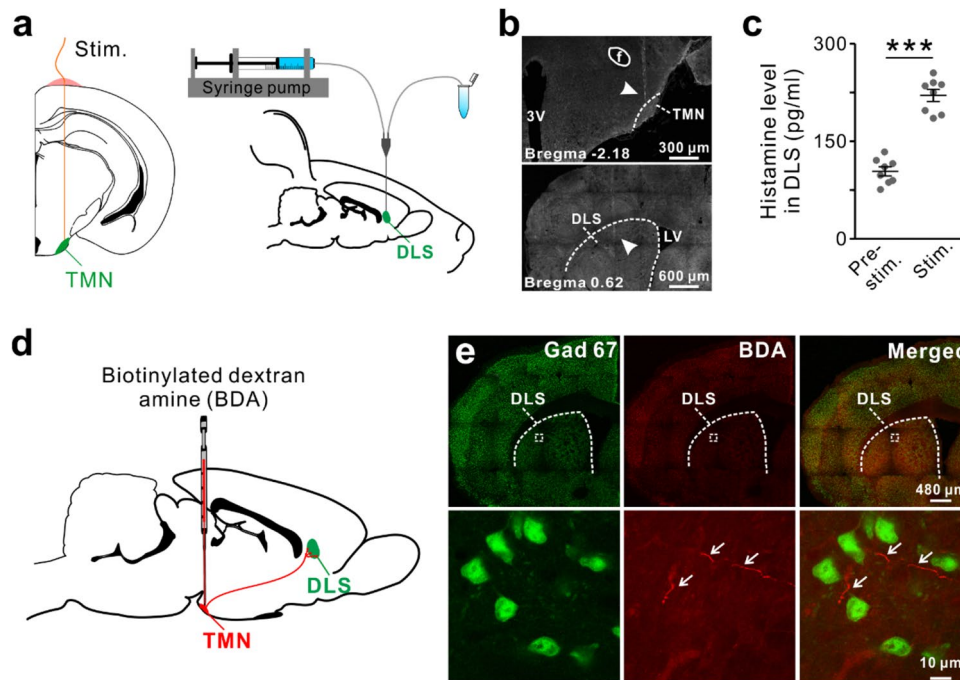


**Fig. 1** Histaminergic innervation from TMN to DLS. **a** Diagrams of TMN stimulation and DLS microdialysis. **b** Upper panel: representative coronal brain section taken through the TMN plane, the path of the electrode is indicated by an arrowhead. Lower panel: representative coronal brain section of the DLS, the path of the microdialysis probe is indicated by an arrowhead. **c** ELISA analyses revealed the level of histamine (pg/mL of tissues) in the microdialysis sample before and during TMN stimulation in DLS ( $n=8$  mice, two-tailed

paired  $t$ -test;  $t_7 = -35.509$ ;  $P < 0.001$ ). **d** Diagram of biotinylated dextran amine (BDA) injection into the TMN. **e** Double immunostainings revealed the GABAergic neurons and histaminergic fibers in the DLS; note that these histaminergic fibers passed around Gad67 immunoreactive (GABAergic) neurons in the DLS as indicated by arrowheads (3 independent experiments). TMN, tuberomammillary nucleus; LV, lateral ventricle; 3 V, 3rd ventricle; f, fornix. Data are represented as the mean  $\pm$  SEM; \*\*\*  $P < 0.001$

nerve fiber terminals exist in the form of varicosities, it is suggested that histaminergic neurons in the TMN send their fibers directly to the DLS and release histamine to influence the activities of the GABAergic DLS neurons.

### Postsynaptic Efficacy Component Underlying the Histamine-Induced Excitation on DLS Neurons

We first labeled d-SPNs or i-SPNs by injecting Cre-dependent AAV into the DLS of D1 or D2-Cre mice, followed by whole-cell patch-clamp recordings on the brain slices to examine whether histamine directly influenced the activity of d-SPNs or i-SPNs. Of all the identified and recorded 10 d-SPNs (Fig. 2a, b) or i-SPNs (Fig. 2e, f), the bath application of histamine-induced an inward current in all recorded neurons (Fig. 2c, d, g, and h). As shown in Fig. 2d and h, perfusing the slices with ACSF containing TTX (0.3  $\mu$ M), 0.03, 0.1, 0.3, 1, 3, and 10  $\mu$ M histamine elicited a concentration-related inward current on d-SPNs ( $1.78 \pm 0.23$  pA,  $6.91 \pm 0.86$  pA,  $16.33 \pm 0.89$  pA,  $25.05 \pm 1.39$  pA,  $37.86 \pm 0.98$  pA,  $46.51 \pm 1.78$  pA, and  $49.19 \pm 1.82$  pA, respectively; Fig. 2d) and i-SPNs ( $2.04 \pm 0.29$  pA,  $10.93 \pm 1.19$  pA,  $23.77 \pm 1.09$  pA,  $35.44 \pm 1.19$  pA,

$46.1 \pm 1.29$  pA,  $51.81 \pm 1.6$  pA, and  $55.28 \pm 1.9$  pA, respectively; Fig. 2h). Fitting the concentration–response curves yielded the mean concentration of histamine for half-maximal activation (EC<sub>50</sub>) on d-SPNs as 8.95  $\mu$ M (Fig. 2d) and on i-SPNs as 2.79  $\mu$ M (Fig. 2h). These results strongly imply a direct postsynaptic excitatory effect of histamine on the d-SPNs and i-SPNs in DLS.

### Dual Receptor Mechanism Mediated the Postsynaptic Excitatory Effect of Histamine on the DLS Neurons

As is already known, histamine exerts its action via four subtypes of a distinct receptor, including the postsynaptic H<sub>1</sub>R, H<sub>2</sub>R, and H<sub>4</sub>R, and the presynaptic H<sub>3</sub>R [1–3, 28, 29]. Therefore, in the present study, we first employed selective H<sub>1</sub>R, H<sub>2</sub>R, and H<sub>4</sub>R antagonists and agonists to examine which postsynaptic histamine receptor(s) mediated the histamine-induced excitation on the DLS neurons.

In the presence of TTX (0.3  $\mu$ M), the histamine (10  $\mu$ M)-induced inward current was partially blocked by the application of mepyramine (0.3–1  $\mu$ M), which is a highly selective antagonist for H<sub>1</sub>R, from  $54.5 \pm 4.9$  to  $42 \pm 3.21$  pA and  $23.5 \pm 2.13$  pA ( $n=8$ ,  $P < 0.01$  and 0.001, respectively;

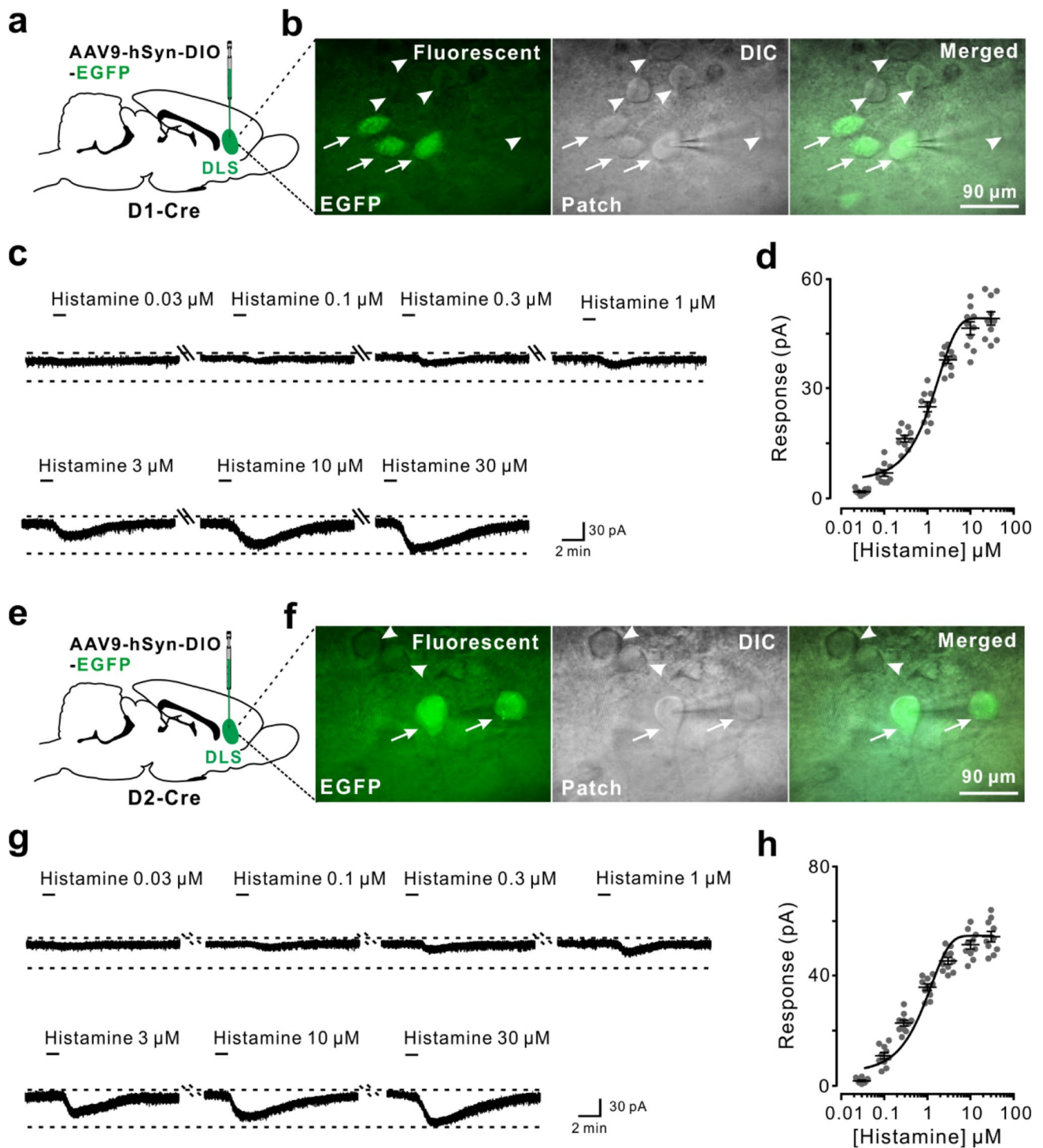


**Fig. 2** Histamine postsynaptically excited d-SPNs and i-SPNs in DLS. **a** The diagram of virus injection in the DLS of D1-Cre mice. **b** Representative fluorescent and DIC field of the coronal brain slice showing d-SPNs labeled with EGFP and the DLS neurons 3 weeks after virus injection during patch-clamp recordings. **c** Histamine (0.03–30  $\mu$ M) induced inward current on recorded d-SPNs in a dose-dependent manner. **d** Concentration–response curves for histamine on

the recorded 10 d-SPNs. **e** The diagram of virus injection in the DLS of the D2-Cre mice. **f** Representative fluorescent and DIC field of a coronal brain slice showing i-SPNs labeled with EGFP and the DLS neurons three weeks after virus injection during patch-clamp recordings. **g** Histamine (0.03–30  $\mu$ M) induced inward current on recorded i-SPNs in a dose-dependent manner. **h** Concentration–response curves for histamine on the recorded 10 i-SPNs



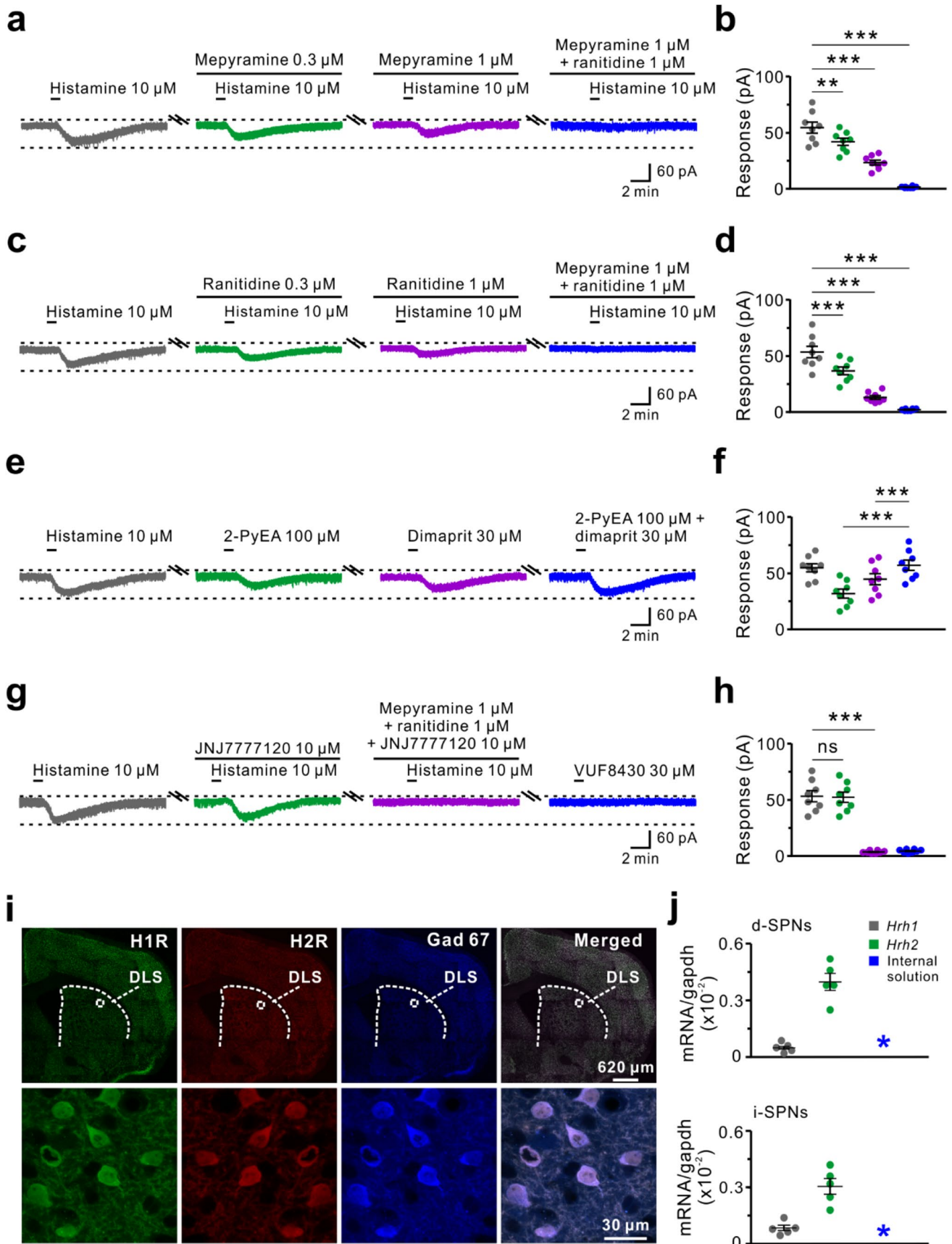




**Fig. 3** Histamine H1R and H2R co-mediated the postsynaptic excitation induced by histamine on the d-SPNs and i-SPNs in DLS. **a** The effect of highly selective H1R antagonist mepyramine (0.3–1  $\mu\text{M}$ ) and mepyramine (1  $\mu\text{M}$ ) together with highly selective H2R antagonist ranitidine (1  $\mu\text{M}$ ) on the inward current elicited by histamine (10  $\mu\text{M}$ ) in the same DLS neuron. **b** Group data of 8 tested DLS neurons (one-way RM-ANOVA;  $F_{(3,21)}=98.186$ ,  $P<0.001$ ; post hoc SNK comparison test). **c** The effect of ranitidine (0.3–1  $\mu\text{M}$ ) and ranitidine (1  $\mu\text{M}$ ) together with mepyramine (1  $\mu\text{M}$ ) on the inward current elicited by histamine (10  $\mu\text{M}$ ) in the same DLS neuron. **d** Group data of 8 tested DLS neurons (one-way RM-ANOVA;  $F_{(3,21)}=93.137$ ,  $P<0.001$ ; post-hoc SNK comparison test). **e** The effect of highly selective H1R agonist 2-PyEA (100  $\mu\text{M}$ ) and H2R agonist dimaprit (30  $\mu\text{M}$ ), and co-application of 2-PyEA (100  $\mu\text{M}$ ) and dimaprit (30  $\mu\text{M}$ ) mimicked the inward current elicited by histamine (10  $\mu\text{M}$ ) in the same DLS neuron. **f** Group data of the 8 tested DLS neurons (one-way RM-ANOVA;  $F_{(3,21)}=189.558$ ,  $P<0.001$ ; post hoc SNK comparison test). **g** The effect of highly selective H4R antagonist JNJ7777120 (10  $\mu\text{M}$ ) and JNJ7777120 (10  $\mu\text{M}$ ) together with mepyramine (0.3  $\mu\text{M}$ ) and ranitidine (0.3  $\mu\text{M}$ ) on the inward current elicited by histamine (10  $\mu\text{M}$ ), and the effect of highly selective H4R agonists VUF8430 (30  $\mu\text{M}$ ) on the same DLS neuron. **h** Group data of the tested 8 DLS neurons (one-way RM-ANOVA;  $F_{(3,21)}=73.663$ ,  $P<0.001$ ; post hoc SNK comparison test). **i** Triple immunostaining revealed that histamine H1R and H2R were co-expressed on the same GABAergic DLS neuron (3 independent experiments), DLS, the dorsolateral striatum. **j** Single-cell qPCR showing the co-expression of *Hrh1* and *Hrh2* mRNAs in d-SPNs and i-SPNs of DLS, asterisks indicate samples depicting no specific signal ( $n=5$  neurons). Data are presented as mean  $\pm$  SEM; ns, no statistical difference, \*\*  $P<0.01$  and \*\*\*  $P<0.001$

Fig. 3a, b), while the combined application of mepyramine (1  $\mu\text{M}$ ) and ranitidine (0.3  $\mu\text{M}$ ) almost totally blocked the inward current evoked by histamine from  $54.5 \pm 4.9$  to  $1.63 \pm 0.26$  pA ( $n=8$ ,  $P<0.001$ ; Fig. 3a, b). On the other hand, the histamine (10  $\mu\text{M}$ )-induced inward current was partially blocked by the application of ranitidine (0.3–1  $\mu\text{M}$ ), a highly selective antagonist for H2R, from  $53.38 \pm 5.1$  to  $36.63 \pm 3.36$  pA and  $13 \pm 1.62$  pA ( $n=8$ ,  $P<0.001$ , respectively; Fig. 3c, d), while the combined application of mepyramine (1  $\mu\text{M}$ ) and ranitidine (1  $\mu\text{M}$ ) almost totally blocked the inward current evoked by histamine from  $53.38 \pm 5.1$  to  $2 \pm 0.33$  pA ( $n=8$ ,  $P<0.001$ ; Fig. 3c, d). Moreover, the inward current induced by histamine was mimicked by 2-PyEA (100  $\mu\text{M}$ ), a highly selective agonist for H1R, and dimaprit (30  $\mu\text{M}$ ), a highly selective agonist for H2R, and co-application of 2-PyEA (100  $\mu\text{M}$ ) and dimaprit (30  $\mu\text{M}$ ) increased the responses, from  $31.75 \pm 3.97$  pA and  $44.63 \pm 4.88$  pA to  $57 \pm 4.59$  pA ( $n=8$ ,  $P<0.001$ , respectively; Fig. 3e, f). Furthermore, JNJ7777120 (10  $\mu\text{M}$ ), a highly selective antagonist for H4R, showed no effect on histamine (10  $\mu\text{M}$ )-induced inward current, from  $53.25 \pm 4.96$  to  $52.38 \pm 4.55$  pA ( $n=8$ ,  $P>0.05$ ; Fig. 3g, h), while the combined application of JNJ7777120 (10  $\mu\text{M}$ ), mepyramine (1  $\mu\text{M}$ ), and ranitidine (1  $\mu\text{M}$ ) almost totally antagonized the inward current evoked by histamine from  $53.25 \pm 4.96$  to  $3.38 \pm 0.42$  pA ( $n=8$ ,  $P<0.001$ ; Fig. 3g, h). And VUF8430

(30  $\mu\text{M}$ ), which is a highly selective agonist for H4R, did not mimic the histamine-induced postsynaptic excitation on the DLS neurons ( $n=8$ ,  $4.25 \pm 0.53$  pA) (Fig. 3g, h). In addition, no difference was noted in the receptor mechanisms between d-SPNs ( $n=14$ ) and i-SPNs ( $n=18$ ).

We next used triple immunostaining experiments to map the distribution of H1R and H2R on the DLS GABAergic neurons, and the results demonstrated that H1R and H2R were co-localized with GABAergic DLS neurons (Fig. 3i). To further assess the expression of *Hrh1* and *Hrh2* mRNAs in the DLS, single-cell qPCR was employed on d-SPNs and i-SPNs ( $n=5$ , respectively). After patch-clamp recordings, the isolated d-SPNs and i-SPNs were screened for the expression of *Hrh1* and *Hrh2* mRNAs. As shown in Fig. 3j, *Hrh1* and *Hrh2* mRNAs co-expressed in d-SPNs and i-SPNs. These results cumulatively indicated a dual receptor mechanism involving H1R and H2R underlying the histamine-induced postsynaptic excitation in DLS neurons.

#### Activation of Presynaptic H3R Suppressed Neuronal Activity by Inhibiting Glutamatergic Synaptic Transmission on DLS Neurons

We further determined the role of presynaptic H3R on DLS neurons through whole-cell patch clamp recording. Our results revealed that application of potent and standard H3R agonist RAMH (10  $\mu\text{M}$ ) could significantly decrease the frequency (from  $3.47 \pm 0.29$  to  $1.74 \pm 0.18$  Hz,  $n=10$ ,  $P<0.001$ ) of sEPSCs on DLS neurons without affecting their amplitudes (from  $12.65 \pm 1.17$  to  $12.64 \pm 1.12$  pA,  $n=10$ ,  $P>0.05$ ) (Fig. 4a–c), application of the potent and selective H3R antagonist IPP (1  $\mu\text{M}$ ) prevented the effect of RAMH (10  $\mu\text{M}$ ) (frequency: from  $3.47 \pm 0.29$  to  $3.43 \pm 0.26$  Hz,  $n=10$ ,  $P>0.05$ ; amplitude: from  $12.65 \pm 1.17$  to  $12.28 \pm 1.07$  pA,  $n=10$ ,  $P>0.05$ ) (Fig. 4a–c), while the co-application of NBQX (10  $\mu\text{M}$ ) and D-AP5 (20  $\mu\text{M}$ ), potent and selective antagonists for AMPA and NMDA receptors, respectively, abolished both the frequency (from  $3.47 \pm 0.29$  to  $0.19 \pm 0.02$  Hz,  $n=10$ ,  $P<0.001$ ) and amplitude (from  $12.65 \pm 1.17$  to  $1.04 \pm 0.11$  pA,  $n=10$ ,  $P<0.001$ ) of sEPSCs on DLS neurons (Fig. 4a–c). These results indicated that activation of H3R inhibits glutamatergic synaptic transmission on DLS neurons. Moreover, neither RAMH (10  $\mu\text{M}$ ) nor RAMH (10  $\mu\text{M}$ ) together with IPP (1  $\mu\text{M}$ ) could affect the frequency (from  $5.47 \pm 0.34$  to  $5.5 \pm 0.38$  Hz and  $5.41 \pm 0.36$  Hz,  $n=10$ ,  $P>0.05$ , respectively) and amplitude (from  $40.86 \pm 2.25$  to  $40.48 \pm 2.25$  pA and  $40.59 \pm 2.15$  pA,  $n=10$ ,  $P>0.05$ , respectively) of sIPSC on DLS neurons (Fig. 4d–f), as well as application of SR95531 (10  $\mu\text{M}$ ), a competitive and selective GABA<sub>A</sub> antagonist, abolished both the frequency (from  $5.47 \pm 0.34$  to  $0.21 \pm 0.03$  Hz,  $n=10$ ,  $P<0.001$ ) and amplitude (from  $40.86 \pm 2.25$  to  $1.88 \pm 0.21$  pA,  $n=10$ ,  $P<0.001$ ) of sIPSC

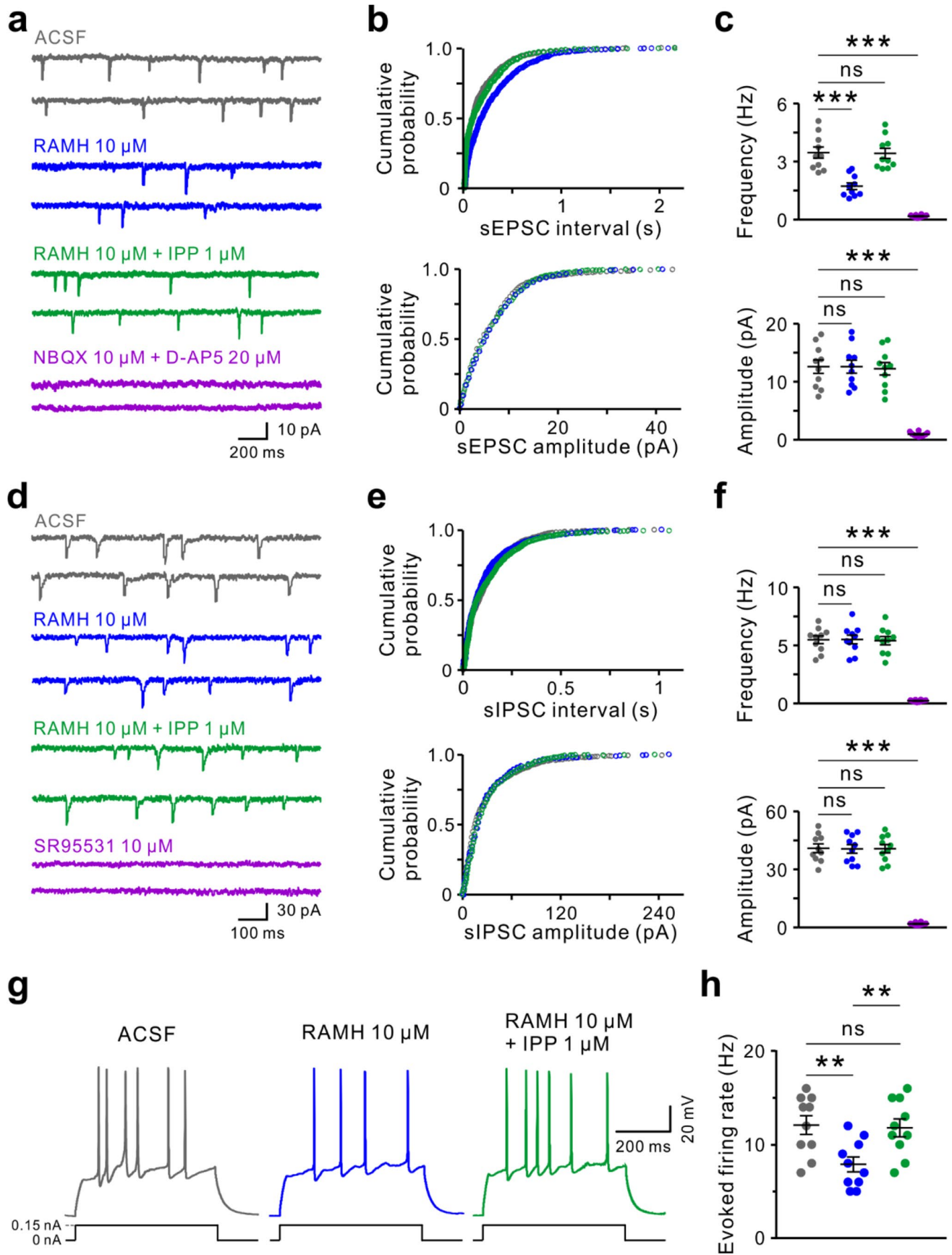


**Fig. 4** H3R activation suppressed neuronal activity by inhibiting glutamatergic rather than GABAergic synaptic transmission on DLS neurons. **a** Raw current traces of sEPSCs recorded in DLS neurons in ACSF, application of selective histamine H3R agonist RAMH (10  $\mu$ M), co-application of RAMH (10  $\mu$ M) and selective H3 receptor antagonist IPP (1  $\mu$ M), co-application of NBQX (10  $\mu$ M) and D-AP5 (20  $\mu$ M) in the presence of SR95531 (10  $\mu$ M). **b** Cumulative distributions of sEPSC intervals and amplitudes for the DLS neurons illustrated in **a**. **c** Group data of the average sEPSC frequency ( $n=10$  neurons, one-way RM-ANOVA, post hoc SNK comparison test,  $F_{(3, 27)}=131.037$ ,  $P<0.001$ ) and amplitude ( $n=10$  neurons, one-way RM-ANOVA, post hoc SNK comparison test,  $F_{(3, 27)}=98.023$ ,  $P<0.001$ ) on the tested DLS neurons. **d** Raw current traces of sIPSCs recorded in DLS neurons in ACSF, application of RAMH (10  $\mu$ M), co-application of RAMH (10  $\mu$ M) and IPP (1  $\mu$ M), and application of SR95531 (10  $\mu$ M) in the presence of NBQX (10  $\mu$ M) and D-AP5 (20  $\mu$ M). **e** The cumulative distributions of neuronal sIPSCs intervals and amplitudes illustrated in **d**. **f** Group data of the average sIPSC frequency ( $n=10$  neurons, one-way RM-ANOVA, post hoc SNK comparison test,  $F_{(3, 27)}=203.124$ ,  $P<0.001$ ) and amplitude ( $n=10$  neurons, one-way RM-ANOVA, post hoc SNK comparison test,  $F_{(3, 27)}=294.38$ ,  $P<0.001$ ) on the tested DLS neurons. **g** The effects of RAMH (10  $\mu$ M) and RAMH (10  $\mu$ M) together with IPP (10  $\mu$ M) on evoked firing of DLS neurons. **h** Group data of the 10 tested DLS neurons ( $n=10$  neurons, one-way RM-ANOVA;  $F_{(2, 18)}=8.221$ ,  $P=0.003$ ; post hoc SNK comparison test). Data are presented as mean  $\pm$  SEM; ns, no statistical difference, \*\* $P<0.01$  and \*\*\* $P<0.001$

on DLS neurons (Fig. 4d–f). These results indicated that activation of H3R had no effect on GABAergic synaptic transmission on DLS neurons. Furthermore, in current-clamp mode, application of RAMH (10  $\mu$ M) suppressed the number of action potentials evoked via positive current stimulation (from  $12.1 \pm 1.0$  to  $7.9 \pm 0.8$  Hz,  $n=10$ ,  $P<0.01$ ) on DLS neurons (Fig. 4g, h), while co-application of RAMH (10  $\mu$ M) and IPP (1  $\mu$ M) prevented this inhibitory effect (from  $12.1 \pm 1.0$  to  $11.8 \pm 0.95$  Hz,  $n=10$ ,  $P<0.01$ ) (Fig. 4g, h), indicating activation of the presynaptic H3R suppressed the firing activity of DLS neurons. In addition, the effect of H3R activation did not differ between d-SPNs ( $n=17$ ) and i-SPNs ( $n=13$ ). Taken together, these results suggested that activation of the presynaptic H3R suppressed neuronal activity by inhibiting glutamatergic instead of GABAergic synaptic transmission on DLS neurons.

### Downstream Ionic Mechanisms Linked to H1R

Considering the findings of the dual receptor mechanisms underlying histamine-induced postsynaptic inward current on the DLS neurons, we evaluated the ionic basis underlying the excitation of the DLS neurons induced by histamine by employing 2-PyEA to separate the current. As shown in Fig. 5a, b, the inward current induced by 2-PyEA (100  $\mu$ M) was nearly totally blocked by the application of mepyramine (1  $\mu$ M) from  $33.25 \pm 2.91$  to  $2.5 \pm 0.5$  pA ( $n=8$ ,  $P<0.001$ ).

Past studies have demonstrated various ionic mechanisms coupled to H1R in different brain regions, including

sodium-calcium exchanger (NCX) and potassium channels [1, 30]. Therefore, we first applied SEA0400, a potent blocker for NCXs, to the DLS neurons. As shown in Fig. 5c, d, the 2-PyEA (100  $\mu$ M)-induced inward current was partially abolished by SEA0400 (10  $\mu$ M) from  $34.75 \pm 2.49$  to  $20.63 \pm 1.86$  pA ( $n=8$ ,  $P<0.001$ ), indicating the participation of NCXs in the mediation of excitation of the DLS neurons induced by the activation of H1R. We also applied  $Ba^{2+}$ , a broad-spectrum blocker of the potassium channels, to the DLS neurons. As shown in Fig. 5e, f, the 2-PyEA (100  $\mu$ M)-induced inward current was partially abolished by  $BaCl_2$  (1 mM) from  $33 \pm 2.8$  to  $23.63 \pm 2.53$  pA ( $n=8$ ,  $P<0.001$ ), indicating the involvement of potassium channels on the inward current induced by H1R in the DLS.

Moreover, to evaluate the subtype of potassium channels that mediate 2-PyEA on the DLS neurons, under the condition of NCX blockage by applying SEA0400 (10  $\mu$ M), we conducted slow ramp command tests to obtain the  $I$ - $V$  curves in the absence and presence of 2-PyEA (100  $\mu$ M). The results revealed that the differential current had a reversal potential of  $-105$  mV, near the calculated  $E_k$  (Fig. 6a). We then fitted the curves by subtracting the 2-PyEA currents with the control currents and found that the potassium ion-mediated current had good linearity ( $R^2=0.99$ ) over the tested voltage range (Fig. 6b). Considering that the slow depolarization was associated with an inward current in the presence of SEA0400 (10  $\mu$ M) (Fig. 5c, d), it was confirmed that the closing of potassium leak channels was linked to the inward current induced by 2-PyEA on the DLS neurons. Furthermore, as shown in Fig. 6c, d, the combined application of SEA0400 (10  $\mu$ M) and  $BaCl_2$  (1 mM) almost totally blocked the 2-PyEA-elicited inward current ( $n=8$ , from  $33.25 \pm 3.27$  to  $1.5 \pm 0.33$  pA,  $P<0.001$ ) on the DLS neurons. Since the activated electrogenic NCXs allowed 3  $Na^+$  to enter in exchange for 1  $Ca^{2+}$  going out of the cell, we further evaluated the effect of replacing the external  $Na^+$  with equimolar concentrations of  $Tris^+$ , a relatively high molecular weight organic cation that does not pass through sodium channels, to evaluate sodium-dependent ionic mechanisms on 2-PyEA-induced inward current. As shown in Fig. 6e, f, the replacement of external  $Na^+$  with  $Tris^+$  totally blocked the 2-PyEA (100  $\mu$ M)-induced inward current in the presence of  $BaCl_2$  (1 mM) ( $n=8$ , from  $30.88 \pm 3.66$  pA to  $1.38 \pm 0.18$  pA,  $P<0.001$ ), which confirms that the closing of NCXs was linked to the inward current induced by 2-PyEA on the DLS neurons. In addition, no difference was noted in the ionic mechanisms coupled to H1R between d-SPNs ( $n=20$ ) and i-SPNs ( $n=25$ ). All these results suggest a dual-ionic mechanism, including activating NCXs and closing potassium leak channels coupled to H1R activation in DLS neurons.

Three NCX subtypes (i.e., NCX1, NCX2, and NCX3) were identified, and all were expressed in the brain [31, 32].

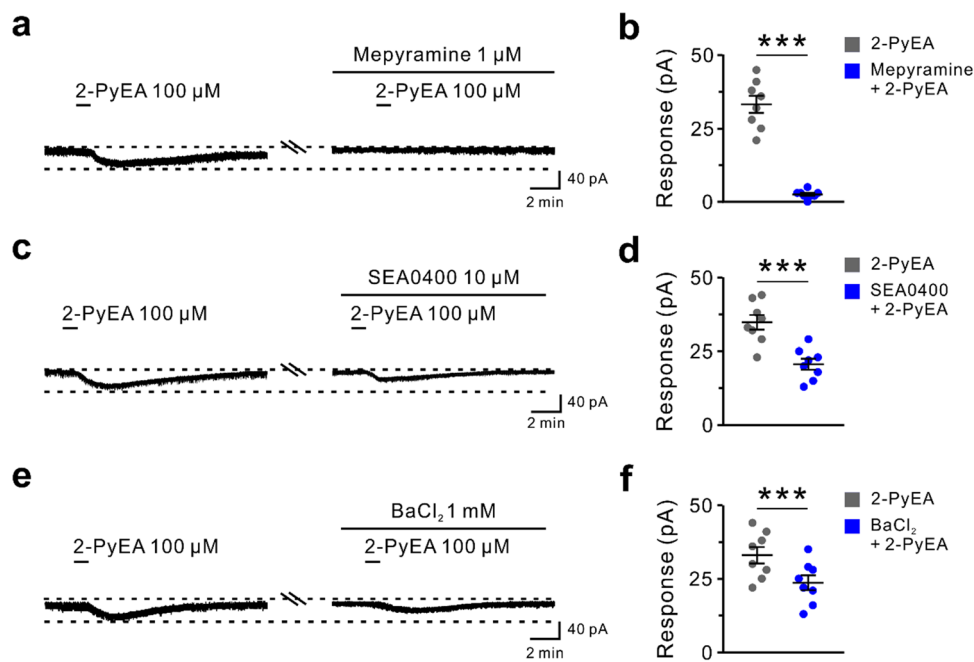


**Fig. 5** NCXs and potassium channels coupled to H1R in the DLS neurons. **a** The effect of mepyramine (1  $\mu$ M) on the inward current induced by 2-PyEA (100  $\mu$ M) in the same DLS neuron. **b** Group data of the 8 tested DLS neurons (two-tailed paired  $t$ -test;  $t_7=10.358$ ;  $P=0.00017$ ). **c** The effect of SEA0400 (10  $\mu$ M), a selective blocker for NCXs, on 2-PyEA (100  $\mu$ M) induced inward current in the same DLS neuron. **d** Group data of the 8 tested DLS neurons (two-tailed

paired  $t$ -test;  $t_7=7.651$ ;  $P=0.000121$ ). **e** The effect of BaCl<sub>2</sub> (1 mM), a broad-spectrum blocker of potassium channels, on the 2-PyEA (100  $\mu$ M) as an inward current induced in the same DLS neuron. **f** Group data of the 8 tested DLS neurons (two-tailed paired  $t$ -test;  $t_7=5.691$ ;  $P=0.0008$ ). Data are represented as mean  $\pm$  SEM; \*\*\*  $P < 0.001$

Therefore, to further assess the *Ncx1-3* mRNA expression in the DLS, single-cell qPCR was performed on the d-SPNs and i-SPNs ( $n=5$ , respectively). After patch-clamp recordings, the isolated d-SPNs and i-SPNs were screened for the expression of *Hrh1* and *Ncx1-3* mRNAs. We found *Hrh1* and *Ncx1-3* mRNAs co-expressed on d-SPNs (Fig. 6g) and i-SPNs (Fig. 6h).

We further confirmed the type/types of ion channels coupled with the downstream of H1R by CRISPR/Cas9 gene-editing technology. Considering the abundant relative expression of *Ncx3* mRNA in DLS neurons (Fig. 6g, h), we injected AAV carrying *Ncx3* sgRNA into DLS of LSL-Cas9-tdTomato::D1/D2-Cre mice to selectively knockout the NCX3 subtype on DLS neurons (Fig. 7a). We noted no significant difference in the numerical density of neurons labeled tdTomato and neurons labeled both EGFP and tdTomato ( $n=10$ ,  $P=0.343$ ; Fig. 7b, c), suggesting the selectivity and specificity of NCX3 subtype knockout in the DLS neurons. We next evaluated the effect of selective knockout of NCX3 subtype in the DLS neurons on the neuronal activity mediated by H1R. As shown in Fig. 7d, e, in the presence of BaCl<sub>2</sub> (1 mM), 2-PyEA induced an inward current on the DLS neurons both in saline and the control virus injected mice ( $n=10$ ,  $25.03 \pm 3.09$  pA and  $26.22 \pm 2.85$  pA, respectively,  $P > 0.05$ ), and the inward current induced

by 2-PyEA was almost totally blocked by NCX3 subtype knockout in the DLS neurons from  $26.22 \pm 2.85$  pA in control virus to  $4.45 \pm 0.63$  pA in virus-carrying *Ncx3* sgRNA injected mice ( $n=10$ ,  $P < 0.001$ ). Moreover, as shown in Fig. 7f, g, in current-clamp mode, 2-PyEA (100  $\mu$ M) on evoked firing of DLS neurons did not differ between saline and control virus injected mice ( $n=10$ ,  $9.8 \pm 0.87$  Hz and  $9.2 \pm 0.63$  Hz, respectively,  $P > 0.05$ ), while 2-PyEA (100  $\mu$ M) on evoked firing was reduced by NCX3 subtype knockout in the DLS neurons from  $9.2 \pm 0.63$  Hz in control virus to  $2.5 \pm 0.31$  Hz in virus-carrying *Ncx3* sgRNA injected mice ( $n=10$ ,  $P < 0.001$ ). Furthermore, no difference was noted in the downstream ionic mechanism coupled to H1R and H2R between d-SPNs ( $n=12$ ) and i-SPNs ( $n=8$ ). All these results strongly support that the NCX3 subtype and potassium leak channels coupled to H1R mediated the effect of histamine on DLS neurons.

#### Downstream Ionic Mechanisms Linked to H2R

Past studies have demonstrated that H2R is coupled to the HCN channels, which elicit an  $I_h$  (the hyperpolarization-activated cationic) current [21]. To evaluate the ionic basis underlying the excitation of DLS neurons induced by H2R, we employed an H2R agonist, dimaprit, to isolate the



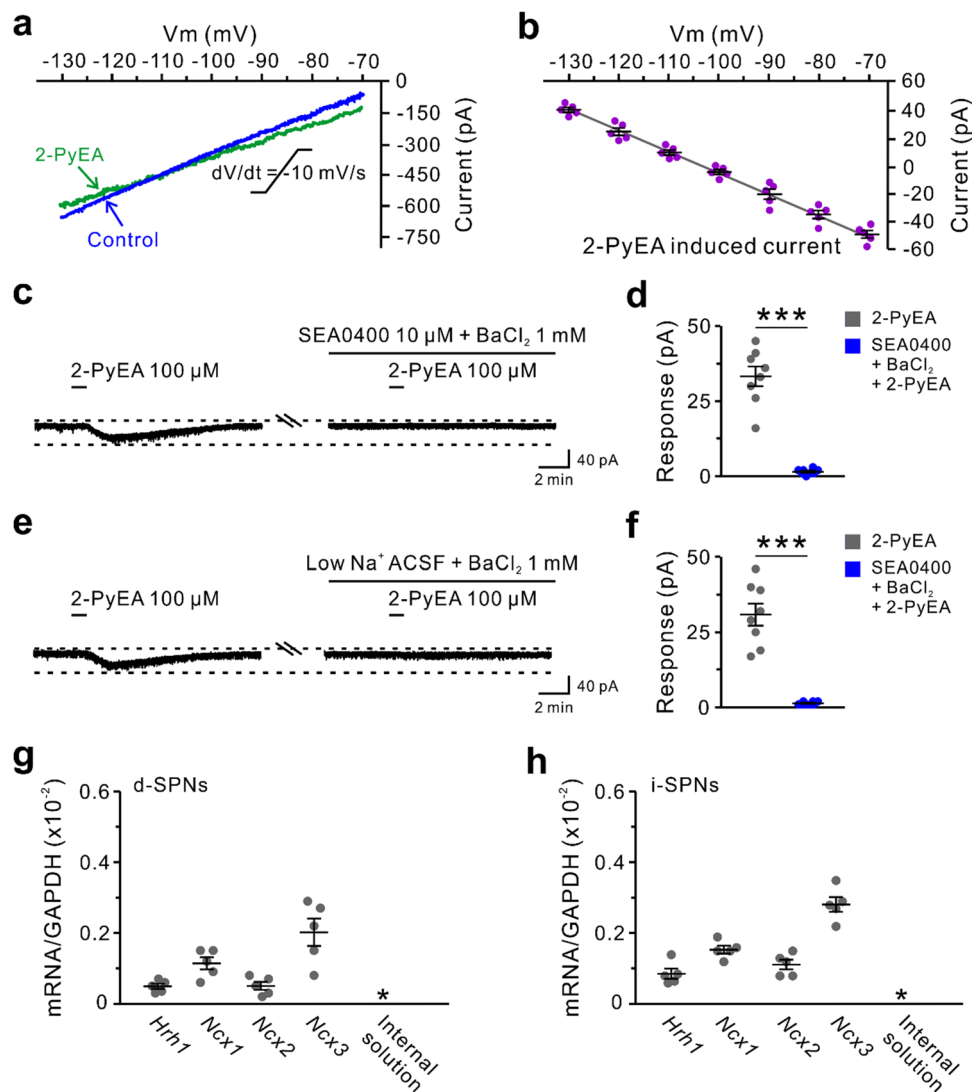


**Fig. 6** NCXs and potassium leak channels coupled to H1R in the DLS neurons. **a** In the ACSF containing SEA0400 (10  $\mu$ M), 2-PyEA-induced changes of  $I$ - $V$  curves of a DLS neuron in slow-ramp command tests ( $dV/dt = -10$  mV/s). **b** Group data of the difference current representing the 2-PyEA-induced current was yielded by subtracting the control from the current recorded during the 2-PyEA application of the 5 tested DLS neurons. **c** The effect of the co-application of KB-R7943 (10  $\mu$ M) and  $BaCl_2$  (1 mM) on the 2-PyEA (100  $\mu$ M) induced inward current in the same DLS neuron. **d** Group

data of the 8 tested DLS neurons (two-tailed paired  $t$ -test;  $t_7 = 10.154$ ;  $P = 0.0000193$ ). **e** The effect of low  $Na^+$  ACSF containing  $BaCl_2$  (1 mM) on the 2-PyEA (100  $\mu$ M) induced inward current in the same DLS neuron. **f** Group data of the 8 tested DLS neurons (two-tailed paired  $t$ -test;  $t_7 = 8.416$ ;  $P = 0.0000658$ ). **g, h** Single-cell qPCR exhibiting the co-expression of *Hrh1* and *Ncx1-3* mRNAs on d-SPNs and i-SPNs. All DLS neurons co-expressed *Hrh1* and *Ncx1-3* mRNAs. Asterisks indicate samples showing no specific signal ( $n = 5$  neurons). Data are represented as mean  $\pm$  SEM; \*\*\* $P < 0.001$

current. As shown in Fig. 8a, b, an inward current induced by dimaprit (30  $\mu$ M) was almost totally blocked by the application of ranitidine (1  $\mu$ M) from  $44.5 \pm 5.0$  pA to  $1.82 \pm 0.37$  pA ( $n = 8$ ,  $P < 0.001$ ). ZD7288 (10  $\mu$ M), a selective antagonist of the HCN channels, totally blocked the inward current induced by dimaprit from  $44.5 \pm 5.0$  to  $3.88 \pm 0.29$  pA ( $n = 8$ ,  $P < 0.001$ ). Moreover, as shown in Fig. 8c, d, an inward current induced by dimaprit (30  $\mu$ M) was not affected by the application of 4-AP (10  $\mu$ M), A-type potassium channel blocker [33], from  $45.13 \pm 4.56$  to  $43.38 \pm 4.11$  pA ( $n = 8$ ,

$P > 0.05$ ), and application of PKA inhibitor H89 (10  $\mu$ M), totally blocked the inward current induced by dimaprit from  $45.13 \pm 4.56$  to  $2.13 \pm 0.29$  pA ( $n = 8$ ,  $P < 0.001$ ), indicating a PKA-mediated action on HCN channels instead of A-type potassium channel coupled to H2R. Furthermore, to further determine the ionic mechanisms underlying H2R, we conducted a series of 1 s hyperpolarizing voltage steps (ranging from  $-70$  to  $-130$  mV in  $-10$  mV steps) to determine the effect of histamine on the HCN channel current (*I<sub>h</sub>*). As shown in Fig. 8e, f, dimaprit (30  $\mu$ M) induced a significant

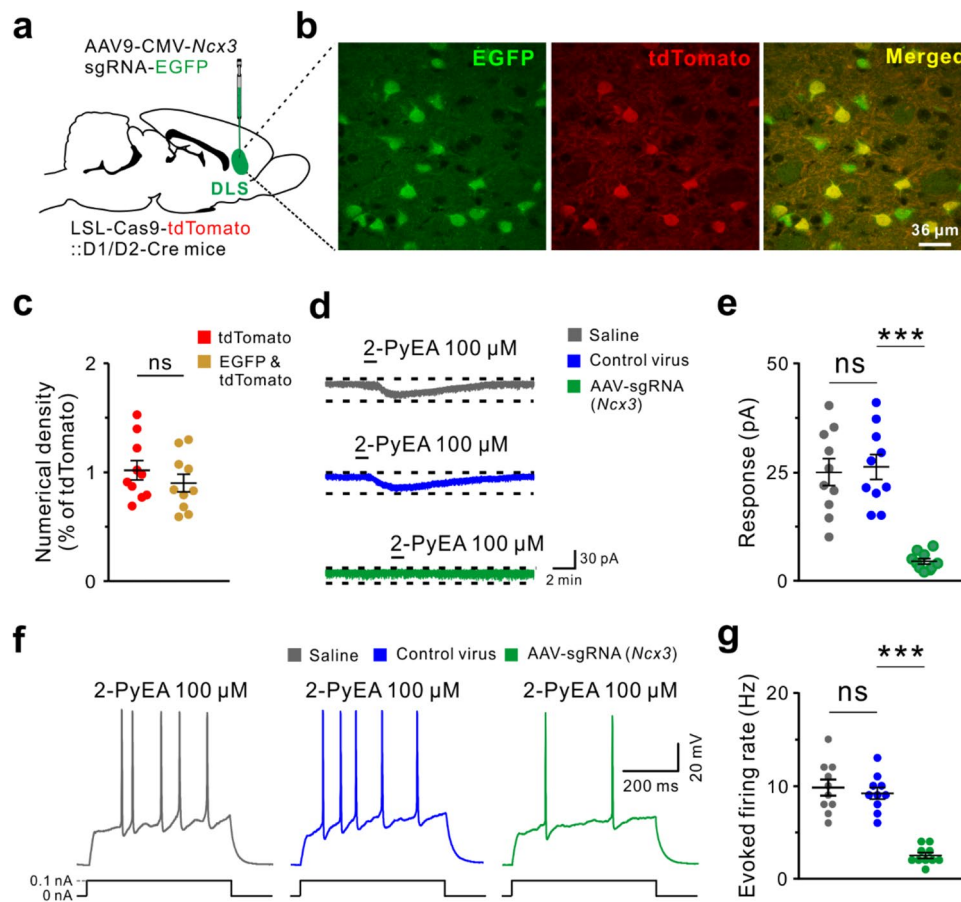


**Fig. 7** NCX3 subtype mediated the effect of HIR activation on DLS neurons. **a** The diagram of virus-carrying *Ncx3* sgRNA injection into the DLS of LSL-Cas9-tdTomato::D1/D2-Cre mice. **b** Representative image of the expression of *Ncx3* sgRNA (green-colored, indicated by EGFP), Cas9 (red-colored, indicated by tdTomato), Cas9, and NCX3 sgRNA co-expression (merged) on the DLS neurons. **c** The relative quantification of neurons expression Cas9 and neurons co-expression of Cas9 and *Ncx3* sgRNA in numerical density ( $n=10$  neurons, two-tailed unpaired  $t$ -test;  $t_{18}=0.975$ ;  $P=0.343$ ). **d** 2-PyEA ( $100\ \mu\text{M}$ ) induced inward current on the DLS neurons in saline, con-

trol virus, and AAV-*Ncx3* sgRNA injected mice in the presence of BaCl<sub>2</sub> ( $1\ \text{mM}$ ). **e** Group data of the 10 tested DLS neurons ( $n=10$  neurons, one-way ANOVA;  $F_{(2,27)}=25.159$ ,  $P<0.001$ ; post hoc SNK comparison test). **f** Effects of 2-PyEA ( $100\ \mu\text{M}$ ) on evoked firing of DLS neurons in saline, control virus, and AAV-*Ncx3* sgRNA injected mice in the presence of BaCl<sub>2</sub> ( $1\ \text{mM}$ ). **g** Group data of the 10 tested DLS neurons ( $n=10$  neurons, one-way ANOVA;  $F_{(2,27)}=39.698$ ,  $P<0.001$ ; post hoc SNK comparison test). Data are presented as mean  $\pm$  SEM; ns, no statistical difference, \*\*\* $P<0.001$

increment in the hyperpolarization-induced HCN channel current ( $I_h$ ) at step potentials  $< -90\ \text{mV}$  ( $P<0.05$ ,  $0.01$ , and  $0.001$ , respectively), and ZD7288 ( $10\ \mu\text{M}$ ) almost totally blocked the hyperpolarization-induced HCN channel current ( $I_h$ ) as well as prevented the increment in the HCN channel current ( $I_h$ ) induced by dimaprit at step potentials  $< -80\ \text{mV}$  ( $n=6$ ,  $P<0.01$  and  $0.001$ , respectively). In addition, no difference was noted in the ionic mechanism coupled to H2R between d-SPNs ( $n=10$ ) and i-SPNs ( $n=11$ ).

We further conducted immunostaining and single-cell RT-PCR analyses to assess whether H2R protein and *Hrh2* mRNAs, along with four subtypes of the HCN channel subtype protein HCN<sub>1-4</sub> and *Hcn1-4* mRNAs, were selectively expressed in the recorded DLS neurons. Immunostaining revealed that all four subtypes of the HCN channel protein

were distributed on the DLS (Fig. 9a). Single-cell qPCR results indicated that the *Hrh2* and *Hcn1-4* mRNA were all expressed on d-SPNs ( $n=5$ , Fig. 9b) and i-SPNs ( $n=5$ , Fig. 9c). All these results strongly imply that the HCN channels underlying the H2R-mediated depolarization on the DLS neurons.

We further confirmed the type/types of ion channels coupled with the downstream of H2R by CRISPR/Cas9 gene-editing technology. Considering the abundant relative expression of *Hcn2* mRNA in DLS neurons (Fig. 9b, c), we injected AAV carrying *Hcn2* sgRNA into DLS of LSL-Cas9-tdTomato::D1/D2-Cre mice to selectively knockout the HCN2 channel on DLS neurons (Fig. 10a). We noted no significant difference in the numerical density of neurons labeled tdTomato and neurons labeled both EGFP

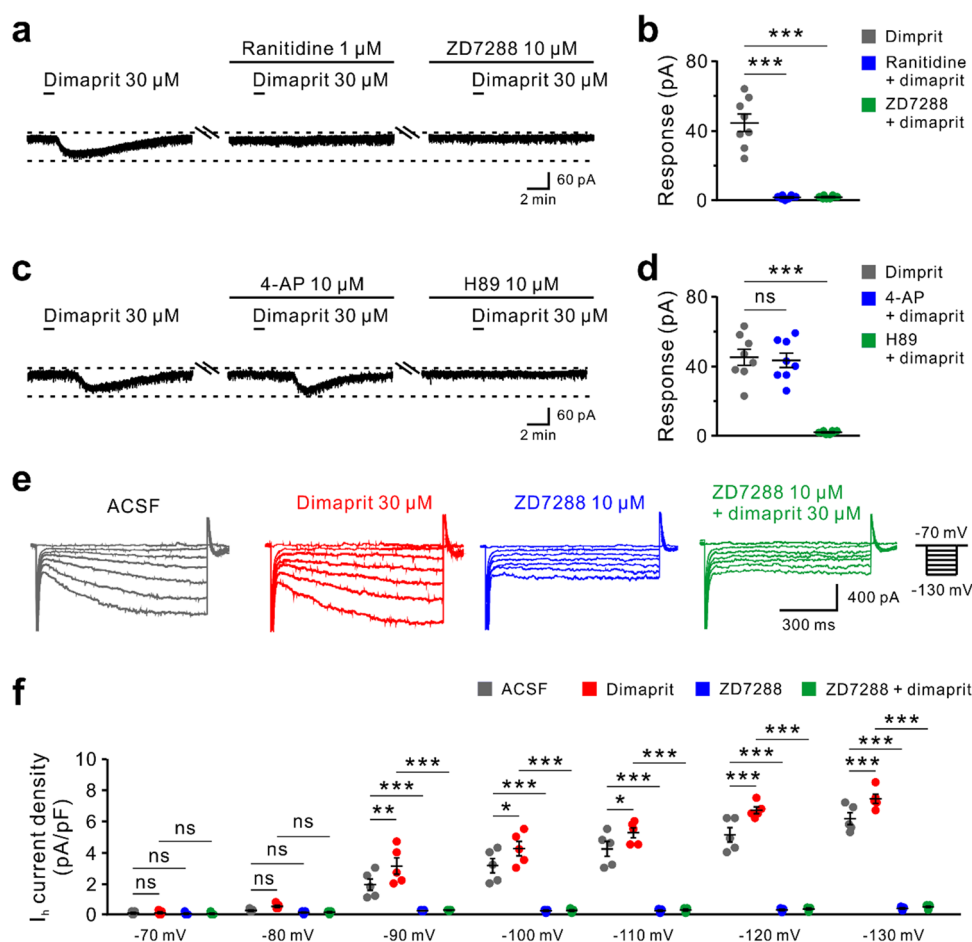


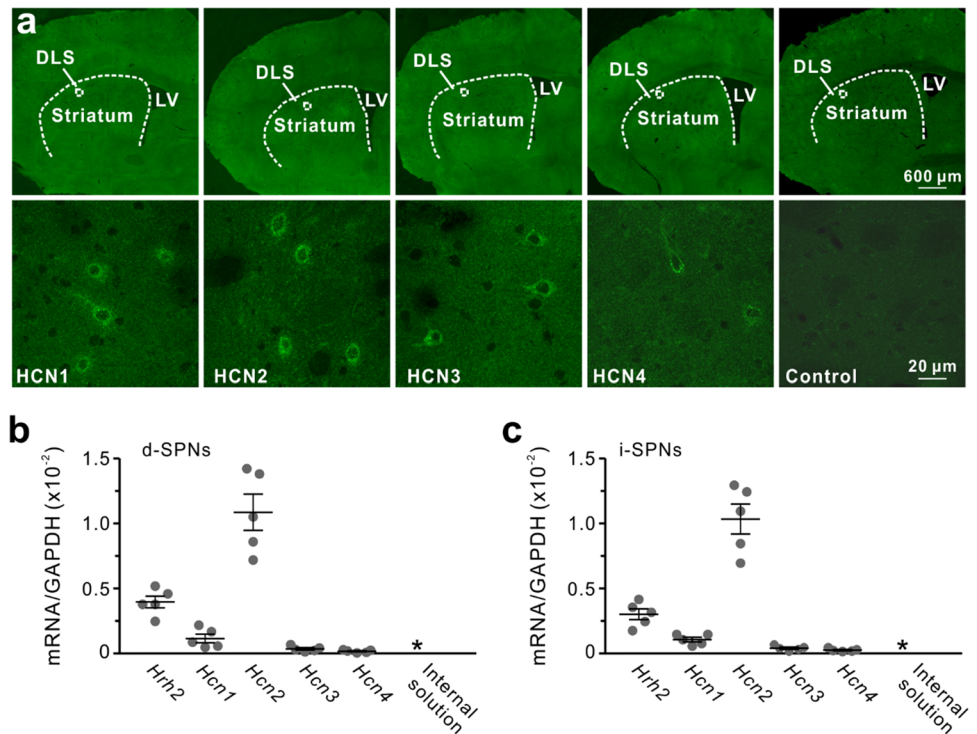
**Fig. 8** HCN channels coupled to H2R in the DLS neurons. **a** The effect of ranitidine (1  $\mu\text{M}$ ) or selective antagonist of the HCN channels ZD7288 (10  $\mu\text{M}$ ) on dimaprit (30  $\mu\text{M}$ ) induced an inward current in the same DLS neuron. **b** Group data of the 8 tested DLS neurons (one-way RM-ANOVA;  $F_{(2,18)}=26.703$ ,  $P<0.001$ ; post hoc SNK comparison test). **c** The effect of A-type potassium channel blocker, 4-AP (10  $\mu\text{M}$ ), and PKA inhibitor H89 (10  $\mu\text{M}$ ) on dimaprit (30  $\mu\text{M}$ ) induced inward current in the same DLS neuron. **d** Group data of the 8 tested DLS neurons (one-way RM-ANOVA;  $F_{(2,18)}=35.552$ ,  $P<0.001$ ; post hoc SNK comparison test). **e** A series of 1 s hyperpolarizing voltage steps (ranging from  $-70$  to  $-130$  mV in  $-10$  mV

steps) were employed to observe the effect of dimaprit (30  $\mu\text{M}$ ), ZD7288 (10  $\mu\text{M}$ ), and dimaprit (30  $\mu\text{M}$ ) together with ZD7288 (10  $\mu\text{M}$ ) on the HCN channel current ( $I_h$ ). **f** Group data of the tested DLS neurons revealed the  $I_h$  current density in the control and during the application of the dimaprit ZD7288 alone and dimaprit together with ZD7288 against the membrane potential from  $-70$  to  $-130$  mV ( $n=5$  neurons; two-way RM-ANOVA; group,  $F_{(6,72)}=111.054$ ,  $P<0.001$ ; treatment,  $F_{(3,72)}=87.285$ ,  $P<0.001$ ; interaction,  $F_{(18,72)}=110.091$ ,  $P<0.001$ ; post hoc SNK comparison test). Data are presented as mean  $\pm$  SEM; ns, no statistical difference, \*  $P<0.05$ , \*\*  $P<0.01$ , and \*\*\*  $P<0.001$

and tdTomato ( $n=10$ ,  $P=0.343$  and  $0.575$ , respectively; Fig. 10b, c), suggesting the selectivity and specificity of HCN2 channel knockout in the DLS neurons. We next evaluated the effect of selective knockout of HCN2 channel in the DLS neurons on the neuronal activity mediated by H2R. As shown in Fig. 10d, e, dimaprit induced an inward current on the DLS neurons both in saline and in the control virus injected mice ( $42.1 \pm 3.38$  pA and  $41.3 \pm 2.19$  pA, respectively,  $n=10$ ,  $P>0.05$ ), and the inward current induced by dimaprit was almost totally blocked by HCN2 channel knockout in the DLS neurons from  $41.3 \pm 2.19$  pA in control virus to  $3.4 \pm 0.4$  pA in virus-carrying *Hcn2* sgRNA injected mice ( $n=10$ ,  $P<0.001$ ).

Moreover, we conducted a series of 1 s hyperpolarizing voltage steps (ranging from  $-70$  to  $-130$  mV in  $-10$  mV steps) to induce the HCN channel current ( $I_h$ ) in the DLS neurons. As shown in Fig. 10f, g, in *Hcn2* sgRNA injected mice, the HCN channel current ( $I_h$ ) of the DLS neurons at step potentials on  $-130$  mV was completely abolished both in the application of normal ACSF (control, from  $6.89 \pm 0.75$  to  $0.36 \pm 0.05$  pA/pF,  $n=10$ ,  $P<0.001$ ) and dimaprit (from  $8.87 \pm 0.77$  to  $0.35 \pm 0.04$  pA/pF,  $n=10$ ,  $P<0.001$ ). Dimaprit induced a significant increment in the HCN channel current ( $I_h$ ) of the DLS neurons at step potentials on  $-130$  mV, from  $6.89 \pm 0.75$  to  $8.87 \pm 0.77$  pA/pF in saline and from  $6.95 \pm 0.75$  to  $8.77 \pm 0.71$  pA/pF in the

**Fig. 9** Distribution and expression of HCN1–4 channel subtypes in the DLS neurons. **a** Antibody staining for HCN1, HCN2, HCN3, and HCN4 channel subtypes in the mouse DLS (3 independent experiments). Negative staining control with the omission of the primary antiserum. LV, lateral ventricle, DLS, the dorsolateral striatum. **b, c** Single-cell qPCR demonstrating the co-expression of *Hrh2* and *Hcn1–4* mRNAs on d-SPNs and i-SPNs. All DLS neurons co-expressed *Hrh2* and *Hcn1–4* mRNAs. Asterisks indicate samples with no specific signal ( $n = 5$  neurons)



control virus injected mice ( $n = 10$ ,  $P < 0.05$ , respectively). On the other hand, in *Hcn2* sgRNA injected mice, dimaprit lost its increasing effect on the HCN channel current (*I<sub>h</sub>*) of the DLS neurons from  $0.36 \pm 0.05$  to  $0.35 \pm 0.04$  pA/pF ( $n = 10$ ,  $P = 0.987$ ). Furthermore, as shown in Fig. 10h, i, in current-clamp mode, dimaprit (30  $\mu\text{M}$ ) on evoked firing of DLS neurons did not differ between saline and control virus injected mice ( $n = 10$ ,  $12.7 \pm 0.84$  Hz and  $11.8 \pm 1.02$  Hz, respectively,  $P > 0.05$ ), while dimaprit (30  $\mu\text{M}$ ) on evoked firing was reduced by HCN2 channel knockout in the DLS neurons from  $11.8 \pm 1.02$  Hz in control virus to  $2.6 \pm 0.4$  Hz in virus-carrying *Hcn2* sgRNA injected mice ( $n = 10$ ,  $P < 0.001$ ). In addition, no difference was noted in the downstream ionic mechanism coupled to H1R and H2R between d-SPNs ( $n = 12$ ) and i-SPNs ( $n = 18$ ). All these results strongly support that the HCN2 channel coupled to H2R mediated the effect of histamine on DLS neurons.

## Discussion

Rodent DLS is a part of the sensorimotor striatum, which integrates glutamatergic innervation from the motor cortex and thalamus and plays an important role in motor control and motor learning [9, 11, 34]. In our earlier report, we have shown that histamine excited rat striatum via both H1R and H2R [5]. In the present study, we demonstrated that the histaminergic innervation from the TMN to DLS (Fig. 1) and histamine excited d-SPNs and i-SPNs in DLS

via postsynaptic H1R and H2R, whereas activation of the presynaptic H3R inhibited the activity of d-SPNs and i-SPNs in DLS at molecular, cellular, and circuitry levels (Figs. 2, 3, and 4). Moreover, using CRISPR/Cas9 gene-editing technology, the NCX3 subtype and potassium leak channels coupled to H1R co-mediated the excitatory effects of histamine (Figs. 5, 6, and 7). Furthermore, through CRISPR/Cas9 gene-editing technology, the HCN2 channel subtype coupled to H2R was found to mediate the effect of histamine on DLS neurons (Figs. 8, 9, and 10). All these results demonstrate the multiple ionic mechanisms underlying the excitatory and inhibitory modulation of the histamine/central histaminergic system on d-SPNs and i-SPNs in mouse DLS, along with the related motor control and motor learning.

Studies have confirmed the expression of H1R, H2R, and H3R in the striatum [5, 19, 35]. H3R is a presynaptic auto- or heteroreceptor, which is highly expressed in the striatum and regulates the release of histamine, glutamate, and dopamine in the striatum through negative feedback [20, 36]. H1R and H2R are postsynaptic receptors, which mediate the excitatory effect of histamine on striatal neurons. Histamine can depolarize isolated rat striatal neurons or cholinergic interneurons of acute striatal slices in vitro in a concentration-dependent manner by acting on either H1R or both H1R and H2R to reduce outward potassium currents [37, 38]. In this study, we demonstrated the excitatory effect of histamine via postsynaptic H1R and H2R, as well as the inhibitory effect of presynaptic H3R activation on d-SPNs and i-SPNs in DLS. These findings are in accordance with



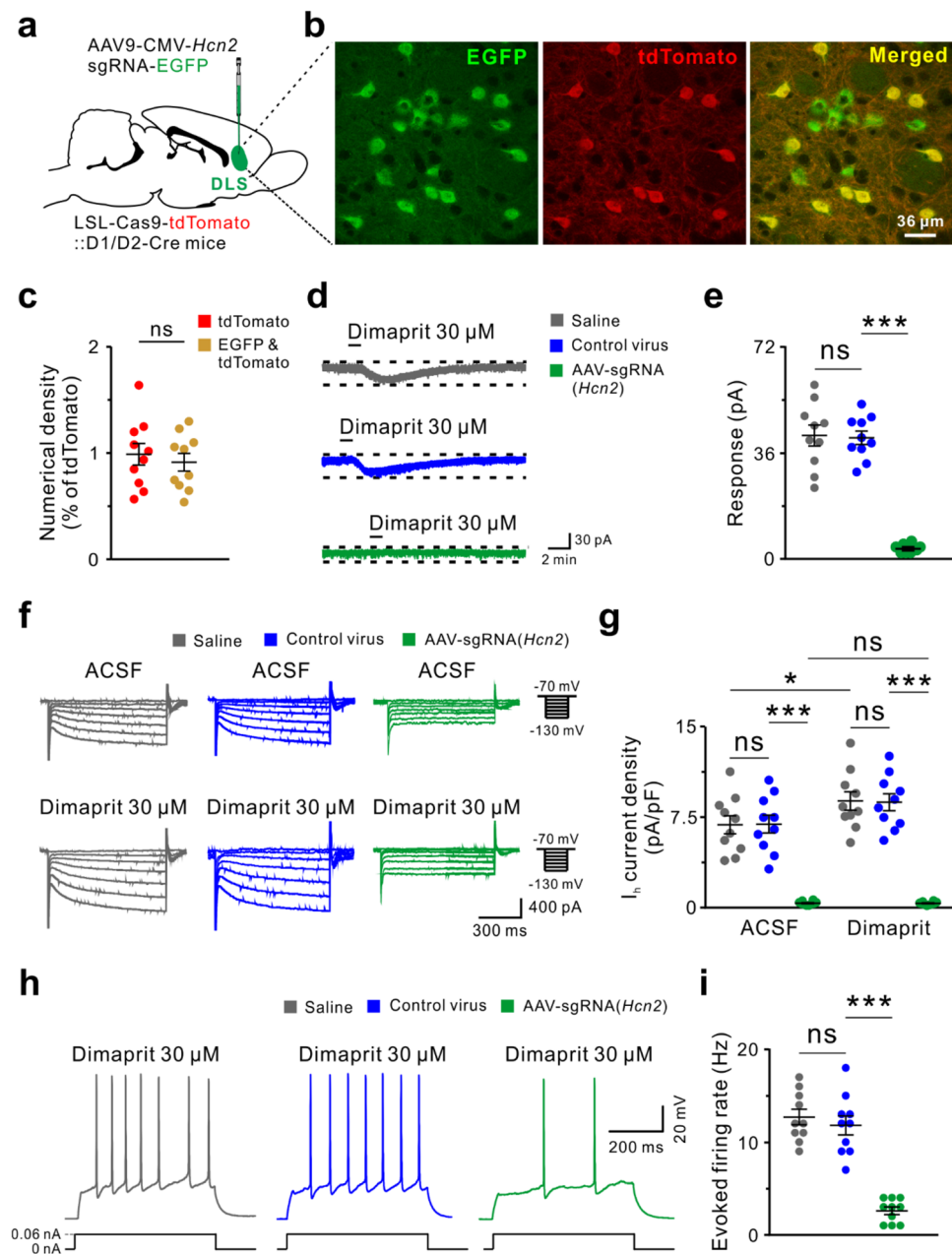


**Fig. 10** HCN2 channel subtype mediated the effect of H2R activation on DLS neurons. **a** Diagram of virus-carrying *Hcn2* sgRNA injection into the DLS of *LSL-Cas9-tdTomato::D1/D2-Cre* mice. **b** Representative image of the expression of *Hcn2* sgRNA (green-colored, indicated by EGFP), Cas9 (red-colored, indicated by tdTomato), Cas9, and *Hcn2* sgRNA co-expression (merged) on the DLS neurons. **c** The relative quantification of neurons expression Cas9 and neurons co-expression of Cas9 and *Hcn2* sgRNA in numerical density ( $n=10$  neurons, two-tailed unpaired *t*-test;  $t_{18}=0.571$ ;  $P=0.575$ ). **d** Dimaprit ( $30\ \mu\text{M}$ ) induced inward current on the DLS neurons in saline, control virus, and AAV-*Hcn2* sgRNA injected mice. **e** Group data of the 10 tested DLS neurons ( $n=10$  neurons, one-way ANOVA;  $F_{(2,27)}=80.342$ ,  $P<0.001$ ; post hoc SNK comparison test). **f** A series of 1 s hyperpolarizing voltage steps (ranging from  $-70$  to  $-130$  mV

in  $-10$  mV steps) were employed to observe the effect of dimaprit ( $30\ \mu\text{M}$ ) on the HCN channel current ( $I_h$ ) in DLS neurons that were selectively knocked out by the HCN2 channel. **g** Group data of the tested DLS neurons indicating the  $I_h$  current density in the control and during the application of dimaprit ( $30\ \mu\text{M}$ ) against the membrane potential on  $-130$  mV ( $n=10$  neurons, two-way RM-ANOVA; group,  $F_{(2,18)}=108.267$ ,  $P<0.001$ ; treatment,  $F_{(1,18)}=5.764$ ,  $P=0.04$ ; interaction,  $F_{(2,18)}=1.719$ ,  $P=0.207$ ; post hoc SNK comparison test). **h** The effects of dimaprit ( $30\ \mu\text{M}$ ) on evoked firing of DLS neurons in saline, control virus, and AAV-*Hcn2* sgRNA injected mice. **i** Group data of the 10 tested DLS neurons ( $n=10$  neurons, one-way ANOVA;  $F_{(2,27)}=49.016$ ,  $P<0.001$ ; post hoc SNK comparison test). Data are presented as mean  $\pm$  SEM; ns, no statistical difference, \* $P<0.05$  and \*\*\* $P<0.001$

the previous in vitro studies involving perforated patch-clamp electrophysiological recordings, immunohistochemical studies as well as in situ hybridization, showing the distribution of histaminergic fibers and receptors in mice, rats, and guinea pigs [5, 20, 38, 39]. Suggesting that the central histaminergic system may modulate the projection neurons in the striatum and subsequently participate in regulating motor control and motor learning, such as parkinsonian motor deficits and cognitive disorders [4, 10, 11].

Previous studies have shown that histamine mediates the excitability of neurons through various signaling pathways downstream of H1R, including phospholipase C-G-protein-IP3 and DAG pathway, potassium leak channels, calcium-activated cation channel, and NCXs [1, 2, 29]. Electrophysiological, in situ hybridization, and immunofluorescence histochemical studies have revealed the distribution of NCX and the expression of potassium leak channels in the basal ganglia [31, 40–42]. In this study, we established that both NCXs and potassium leak channels are involved in the excitation of d-SPNs and i-SPNs in DLS induced by H1R. Since the reversal potential of NCXs is +195 mV, the activation of the antiporter produces a significant depolarization effect [43]. Due to its high capacity and low affinity for sodium and calcium ion transport across the plasma membrane, NCX participates in regulating neuronal firing by reducing the accumulation of calcium ions in neurons [44, 45]. Furthermore, the reversal potential of potassium leak channels is closer to the potassium ion equilibrium potential (−105 mV), which helps in preserving a negative membrane potential and thus decreasing the excitability [41, 46]. Considering that via H1R, histamine excites d-SPNs and i-SPNs in DLS by opening the NCX channel and closing the potassium leakage channel, we speculate that the central histamine can regulate neuronal activities by affecting the intracellular calcium and potassium concentration in DLS neurons.

HCN channel-mediated hyperpolarization-activated mixed cation current ( $I_h$ ) with inward rectification characteristics [47–49]. Immunohistochemistry showed that four types of HCN channels were expressed in rat striatum [50]. In the rat and mouse model of Parkinson's disease (PD), the expression of the HCN channel in cholinergic interneurons in the striatum decreased, resulting in a decrease in  $I_h$  current. This also led to a reduction in neuronal excitability, reduced acetylcholine release, imbalance of dopamine/acetylcholine, and consequently, the emergence of cognitive impairments [51, 52]. In the current work, we could detect the mRNA expression of four types of HCN channels in the d-SPNs and i-SPNs in DLS. Also, histamine excited the d-SPNs and i-SPNs in DLS through the HCN2 channel, coupled downstream of H2R. These results are consistent with the distribution of four types of HCN channel proteins in rat striatum. Furthermore, considering that HCN channels

are closely related to the regularity of neuronal firing rate and firing pattern [21, 53, 54], we speculate that the central histaminergic afferent system may affect motor control and cognitive functions by affecting the neuronal firing activity of d-SPNs and i-SPNs in DLS.

Rodent DLS is part of the sensorimotor striatum, which plays a critical role in controlling motor behavior and cognitive functions [34, 55]. Here, we report the direct excitatory as well as the inhibitory effect of histamine on d-SPNs and i-SPNs in DLS, via postsynaptic H1R and H2R and presynaptic H3R, respectively. Intriguingly, in mice performing an operant task, a transient increase in neuronal activity was observed in d-SPNs and i-SPNs when the animals initiated actions, instead of when they were inactive [56]. DLS NMDA lesions produce apparent deficits in serial reaction time (SRT) of task performance [57]. Patients with PD are impaired in Go/No Go responding, with short response times and accuracy in SRT tasks [58, 59]. Therefore, we need to further validate the role of central histaminergic innervation from the hypothalamus that affects the activity of DLS neurons through its pre- and postsynaptic receptors in motor control and motor learning. Moreover, histamine receptors and ion channels coupled downstream of histamine receptors in d-SPNs and i-SPNs of DLS may be potential targets in the treatment of basal ganglia-related motor diseases such as motor deficits and cognitive impairments.

**Acknowledgements** Thanks to all authors and our colleagues for their contributions to this study.

**Author Contribution** Q.-X. Zhuang conceived and designed the study. J.-Y. Peng, K.-L. Shen, X.-J. Fan, H.-W. Huang, J.-L. Jiang, J.-H. Lu, X.-Q. Wang, X.-X. Fang, and S. Chen performed tracing, immunostaining, single-cell qPCR, and virus injection experiments. Q.-X. Zhuang, X.-J. Fan, W.-R. Yuan, and Q.-X. Deng performed patch-clamp recording experiment. J.-Y. Peng, K.-L. Shen, Z.-X. Qi, and X.-J. Fan involved in ELISA experiment. Q.-X. Zhuang, L. Chen, and Z.-X. Qi analyzed data. Q.-X. Zhuang and L. Chen wrote the paper.

**Funding** This work was supported by the National Natural Science Foundation of China (grants 31771143 and 81702461); Shanghai Municipal Science and Technology Major Project (No.2018SHZDZX01); Shanghai Sailing Program (17YF1426600); Postgraduate Research & Practice Innovation Program of Jiangsu Province (KYCX20\_2820 and KYCX21\_3077); National College Students Innovation and Entrepreneurship Training Program of China (202210304044Z, 202210304125Y and 202110304033Z).

**Data Availability** The datasets analyzed during the current study are available from the corresponding author on reasonable request.

## Declarations

**Ethics Approval** Animal maintenance and experiments were in accordance with the US National Institutes of Health Guide for the Care and Use of Laboratory Animals (NIH Publication 85–23, revised 2011) and were approved by the Institutional Animal Care and Use Committee of Nantong University. All efforts were made to minimize the number of animals used and their suffering.

**Consent to Participate** Not applicable.

**Consent for Publication** Not applicable.

**Conflict of Interest** The authors declare no competing interests.

## References

- Brown RE, Stevens DR, Haas HL (2001) The physiology of brain histamine. *Prog Neurobiol* 63(6):637–672. [https://doi.org/10.1016/S0301-0082\(00\)00039-3](https://doi.org/10.1016/S0301-0082(00)00039-3)
- Haas HL, Sergeeva OA, Selbach O (2008) Histamine in the nervous system. *Physiol Rev* 88(3):1183–1241. <https://doi.org/10.1152/physrev.00043.2007>
- Panula P, Chazot PL, Cowart M, Gutzmer R, Leurs R, Liu WL, Stark H, Thurmond RL, Haas HL (2015) International Union of Basic and Clinical Pharmacology. XCVIII Histamine Receptors. *Pharmacol Rev* 67(3):601–655. <https://doi.org/10.1124/pr.114.010249>
- Hu W, Chen Z (2017) The roles of histamine and its receptor ligands in central nervous system disorders: An update. *Pharmacol Ther* 175:116–132. <https://doi.org/10.1016/j.pharmthera.2017.02.039>
- Zhuang QX, Xu HT, Lu XJ, Li B, Yung WH, Wang JJ, Zhu JN (2018) Histamine excites striatal dopamine D1 and D2 receptor-expressing neurons via postsynaptic H1 and H2 receptors. *Mol Neurobiol* 55(10):8059–8070. <https://doi.org/10.1007/s12035-018-0976-1>
- Zhang J, Zhuang QX, Li B, Wu GY, Yung WH, Zhu JN, Wang JJ (2016) Selective modulation of histaminergic inputs on projection neurons of cerebellum rapidly promotes motor coordination via HCN channels. *Mol Neurobiol* 53(2):1386–1401. <https://doi.org/10.1007/s12035-015-9096-3>
- Soares-Cunha C, Coimbra B, Sousa N, Rodrigues AJ (2016) Reappraising striatal D1- and D2-neurons in reward and aversion. *Neurosci Biobehav Rev* 68:370–386. <https://doi.org/10.1016/j.neubiorev.2016.05.021>
- Tecuapetla F, Jin X, Lima SQ, Costa RM (2016) Complementary contributions of striatal projection pathways to action initiation and execution. *Cell* 166(3):703–715. <https://doi.org/10.1016/j.cell.2016.06.032>
- Makino H, Hwang EJ, Hedrick NG, Komiyama T (2016) Circuit Mechanisms of Sensorimotor Learning. *Neuron* 92(4):705–721. <https://doi.org/10.1016/j.neuron.2016.10.029>
- Grospe GM, Baker PM, Ragozzino ME (2018) Cognitive flexibility deficits following 6-OHDA lesions of the rat dorsomedial striatum. *Neurosci* 374:80–90. <https://doi.org/10.1016/j.neuroscience.2018.01.032>
- Kravitz AV, Matikainen-Ankney BA (2020) Motor control: memory and motor control in the dorsal striatum. *Curr Biol* 30(22):R1366–R1368. <https://doi.org/10.1016/j.cub.2020.09.018>
- Doig NM, Moss J, Bolam JP (2010) Cortical and thalamic innervation of direct and indirect pathway medium-sized spiny neurons in mouse striatum. *J Neurosci* 30(44):14610–14618. <https://doi.org/10.1523/JNEUROSCI.1623-10.2010>
- Chuhma N, Tanaka KF, Hen R, Rayport S (2011) Functional connectome of the striatal medium spiny neuron. *J Neurosci* 31(4):1183–1192. <https://doi.org/10.1523/JNEUROSCI.3833-10.2011>
- Pisani A, Bernardi G, Ding J, Surmeier DJ (2007) Re-emergence of striatal cholinergic interneurons in movement disorders. *Trends Neurosci* 30(10):545–553. <https://doi.org/10.1016/j.tins.2007.07.008>
- Mathur BN, Lovinger DM (2012) Serotonergic action on dorsal striatal function. *Parkinsonism Relat Disord* 18(Suppl 1):S129–131. [https://doi.org/10.1016/S1353-8020\(11\)70040-2](https://doi.org/10.1016/S1353-8020(11)70040-2)
- Lovinger DM (2010) Neurotransmitter roles in synaptic modulation, plasticity and learning in the dorsal striatum. *Neuropharmacol* 58(7):951–961. <https://doi.org/10.1016/j.neuropharm.2010.01.008>
- Romero-Fernandez W, Taura JJ, Crans RAJ, Lopez-Cano M, Fores-Pons R, Narvaez M, Carlsson J, Ciruela F, Fuxe K, Borroto-Escuela DO (2022) The mGlu5 receptor protomer-mediated dopamine d2 receptor trans-inhibition is dependent on the adenosine A2A receptor protomer: implications for Parkinson's disease. *Mol Neurobiol* <https://doi.org/10.1007/s12035-022-02946-9>
- Toval A, Garrigos D, Kutsenko Y, Popovic M, Do-Couto BR, Morales-Delgado N, Tseng KY, Ferran JL (2021) Dopaminergic modulation of forced running performance in adolescent rats: role of striatal D1 and extra-striatal D2 dopamine receptors. *Mol Neurobiol* 58(4):1782–1791. <https://doi.org/10.1007/s12035-020-02252-2>
- Bolam JP, Ellender TJ (2016) Histamine and the striatum. *Neuropharmacol* 106:74–84. <https://doi.org/10.1016/j.neuropharm.2015.08.013>
- Ellender TJ, Huerta-Ocampo I, Deisseroth K, Capogna M, Bolam JP (2011) Differential modulation of excitatory and inhibitory striatal synaptic transmission by histamine. *J Neurosci* 31(43):15340–15351. <https://doi.org/10.1523/JNEUROSCI.3144-11.2011>
- Zhuang QX, Li GY, Li B, Zhang CZ, Zhang XY, Xi K, Li HZ, Wang JJ, Zhu JN (2018) Regularizing firing patterns of rat subthalamic neurons ameliorates parkinsonian motor deficits. *J Clin Invest* 128(12):5413–5427. <https://doi.org/10.1172/JCI99986>
- Paxinos G, Franklin KBJ (2019) The mouse brain in stereotaxic coordinates, 5th edn. Academic Press/Elsevier, San Diego, CA
- Akins VF, Bealer SL (1993) Hypothalamic histamine release, neuroendocrine and cardiovascular responses during tuberomammillary nucleus stimulation in the conscious rat. *Neuroendocrinol* 57(5):849–855. <https://doi.org/10.1159/000126444>
- Weiler HT, Hasenohrl RU, van Landeghem AA, van Landeghem M, Brankack J, Huston JP, Haas HL (1998) Differential modulation of hippocampal signal transfer by tuberomammillary nucleus stimulation in freely moving rats dependent on behavioral state. *Synapse* 28(4):294–301. [https://doi.org/10.1002/\(SICI\)1098-2396\(199804\)28:4<3c294::AID-SYN5%3e3.0.CO;2-4](https://doi.org/10.1002/(SICI)1098-2396(199804)28:4<3c294::AID-SYN5%3e3.0.CO;2-4)
- Wu DC, Zhu-Ge ZB, Yu CY, Fang Q, Wang S, Jin CL, Zhang SH, Chen Z (2008) Low-frequency stimulation of the tuberomammillary nucleus facilitates electrical amygdaloid-kindling acquisition in Sprague-Dawley rats. *Neurobiol Dis* 32(1):151–156. <https://doi.org/10.1016/j.nbd.2008.07.002>
- Aceto G, Nardella L, Nanni S, Pecci V, Bertozzi A, Colussi C, D'Ascenzo M, Grassi C (2022) Activation of histamine type 2 receptors enhances intrinsic excitability of medium spiny neurons in the nucleus accumbens. *J Physiol* 600(9):2225–2243. <https://doi.org/10.1113/JP282962>
- Wang W, Li C, Chen Q, van der Goes MS, Hawrot J, Yao AY, Gao X, Lu C, Zang Y, Zhang Q, Lyman K, Wang D, Guo B, Wu S, Gerfen CR, Fu Z, Feng G (2017) Striatopallidal dysfunction underlies repetitive behavior in Shank3-deficient model of autism. *J Clin Invest* 127(5):1978–1990. <https://doi.org/10.1172/JCI87997>
- Pillot C, Heron A, Cochois V, Tardivel-Lacombe J, Ligneau X, Schwartz JC, Arrang JM (2002) A detailed mapping of the histamine H(3) receptor and its gene transcripts in rat brain. *Neurosci* 114(1):173–193. [https://doi.org/10.1016/S0306-4522\(02\)00135-5](https://doi.org/10.1016/S0306-4522(02)00135-5)
- Haas H, Panula P (2003) The role of histamine and the tuberomammillary nucleus in the nervous system. *Nat Rev Neurosci* 4(2):121–130. <https://doi.org/10.1038/nrn1034>
- McCormick DA, Williamson A (1991) Modulation of neuronal firing mode in cat and guinea pig LGNd by histamine: possible

- cellular mechanisms of histaminergic control of arousal. *J Neurosci* 11(10):3188–3199
31. Canitano A, Papa M, Boscica F, Castaldo P, Sellitti S, Tagliatalata M, Annunziato L (2002) Brain distribution of the Na<sup>+</sup>/Ca<sup>2+</sup> exchanger-encoding genes NCX1, NCX2, and NCX3 and their related proteins in the central nervous system. *Ann N Y Acad Sci* 976:394–404. <https://doi.org/10.1111/j.1749-6632.2002.tb04766.x>
  32. Khananshvil D (2013) The SLC8 gene family of sodium-calcium exchangers (NCX) - structure, function, and regulation in health and disease. *Mol Aspects Med* 34(2–3):220–235. <https://doi.org/10.1016/j.mam.2012.07.003>
  33. Duan KZ, Xu Q, Zhang XM, Zhao ZQ, Mei YA, Zhang YQ (2012) Targeting A-type K(+) channels in primary sensory neurons for bone cancer pain in a rat model. *Pain* 153(3):562–574. <https://doi.org/10.1016/j.pain.2011.11.020>
  34. Yin HH, Knowlton BJ (2006) The role of the basal ganglia in habit formation. *Nat Rev Neurosci* 7(6):464–476. <https://doi.org/10.1038/nrn1919>
  35. Ahmed MR, Jayakumar M, Ahmed MS, Zamaleeva AI, Tao J, Li EH, Job JK, Pittenger C, Ohtsu H, Rajadas J (2019) Pharmacological antagonism of histamine H2R ameliorated L-DOPA-induced dyskinesia via normalization of GRK3 and by suppressing FosB and ERK in PD. *Neurobiol Aging* 81:177–189. <https://doi.org/10.1016/j.neurobiolaging.2019.06.004>
  36. Varaschin RK, Osterstock G, Ducrot C, Leino S, Bourque MJ, Prado MAM, Prado VF, Salminen O, Rannanpää Nee Nuutinen S, Trudeau LE (2018) Histamine H3 receptors decrease dopamine release in the ventral striatum by reducing the activity of striatal cholinergic interneurons. *Neurosci* 376:188–203. <https://doi.org/10.1016/j.neuroscience.2018.01.027>
  37. Bell MI, Richardson PJ, Lee K (2000) Histamine depolarizes cholinergic interneurons in the rat striatum via a H(1)-receptor mediated action. *Br J Pharmacol* 131(6):1135–1142. <https://doi.org/10.1038/sj.bjp.0703692>
  38. Munakata M, Akaike N (1994) Regulation of K<sup>+</sup> conductance by histamine H1 and H2 receptors in neurones dissociated from rat neostriatum. *J Physiol* 480(Pt 2):233–245
  39. Vizuete ML, Traiffort E, Bouthenet ML, Ruat M, Souil E, Tardivel-Lacombe J, Schwartz JC (1997) Detailed mapping of the histamine H2 receptor and its gene transcripts in guinea-pig brain. *Neurosci* 80(2):321–343. [https://doi.org/10.1016/S0306-4522\(97\)00010-9](https://doi.org/10.1016/S0306-4522(97)00010-9)
  40. Jeon D, Chu K, Jung KH, Kim M, Yoon BW, Lee CJ, Oh U, Shin HS (2008) Na<sup>+</sup>/Ca<sup>2+</sup> exchanger 2 is neuroprotective by exporting Ca<sup>2+</sup> during a transient focal cerebral ischemia in the mouse. *Cell Calcium* 43(5):482–491. <https://doi.org/10.1016/j.ceca.2007.08.003>
  41. Wang G, Zeng J, Ren R, Chen S (2008) Potassium channels in the basal ganglia: promising new targets for the treatment of Parkinson's disease. *Front Biosci* 13:3685–3698. <https://doi.org/10.2741/2959>
  42. Singh S, Agarwal P, Ravichandiran V (2021) Two-Pore Domain Potassium Channel in Neurological Disorders. *J Membr Biol* 254(4):367–380. <https://doi.org/10.1007/s00232-021-00189-8>
  43. Wu M, Zaborszky L, Hajszan T, van den Pol AN, Alreja M (2004) Hypocretin/orexin innervation and excitation of identified septohippocampal cholinergic neurons. *J Neurosci* 24(14):3527–3536. <https://doi.org/10.1523/JNEUROSCI.5364-03.2004>
  44. Torrente AG, Zhang R, Zaini A, Giani JF, Kang J, Lamp ST, Philipson KD, Goldhaber JI (2015) Burst pacemaker activity of the sinoatrial node in sodium-calcium exchanger knockout mice. *Proc Natl Acad Sci U S A* 112(31):9769–9774. <https://doi.org/10.1073/pnas.1505670112>
  45. Annunziato L, Secondo A, Pignataro G, Scorziello A, Molinaro P (2020) New perspectives for selective NCX activators in neurodegenerative diseases. *Cell Calcium* 87:102170. <https://doi.org/10.1016/j.ceca.2020.102170>
  46. Dey D, Eckle VS, Vitko I, Sullivan KA, Lasiecka ZM, Winckler B, Stornetta RL, Williamson JM, Kapur J, Perez-Reyes E (2014) A potassium leak channel silences hyperactive neurons and ameliorates status epilepticus. *Epilepsia* 55(2):203–213. <https://doi.org/10.1111/epi.12472>
  47. Biel M, Wahl-Schott C, Michalakis S, Zong X (2009) Hyperpolarization-activated cation channels: from genes to function. *Physiol Rev* 89(3):847–885. <https://doi.org/10.1152/physrev.00029.2008>
  48. Santoro B, Shah MM (2020) Hyperpolarization-activated cyclic nucleotide-gated channels as drug targets for neurological disorders. *Annu Rev Pharmacol Toxicol* 60(60):109–131. <https://doi.org/10.1146/annurev-pharmtox-010919-023356>
  49. Atherton JF, Kitano K, Baufreton J, Fan K, Wokosin D, Tkatch T, Shigemoto R, Surmeier DJ, Bevan MD (2010) Selective participation of somatodendritic HCN channels in inhibitory but not excitatory synaptic integration in neurons of the subthalamic nucleus. *J Neurosci* 30(47):16025–16040. <https://doi.org/10.1523/Jneurosci.3898-10.2010>
  50. Notomi T, Shigemoto R (2004) Immunohistochemical localization of Ih channel subunits, HCN1–4, in the rat brain. *J Comp Neurol* 471(3):241–276. <https://doi.org/10.1002/cne.11039>
  51. Zhao Z, Zhang K, Liu X, Yan H, Ma X, Zhang S, Zheng J, Wang L, Wei X (2016) Involvement of HCN channel in muscarinic inhibitory action on tonic firing of dorsolateral striatal cholinergic interneurons. *Front Cell Neurosci* 10:71. <https://doi.org/10.3389/fncel.2016.00071>
  52. McKinley JW, Shi Z, Kawikova I, Hur M, Bamford IJ, Sudarsana Devi SP, Vahedipour A, Darvas M, Bamford NS (2019) Dopamine deficiency reduces striatal cholinergic interneuron function in models of Parkinson's disease. *Neuron* 103(6):1056–1072 e1056. <https://doi.org/10.1016/j.neuron.2019.06.013>
  53. DiFrancesco JC, DiFrancesco D (2015) Dysfunctional HCN ion channels in neurological diseases. *Front Cell Neurosci* 6:174. <https://doi.org/10.3389/fncel.2015.00071>
  54. Chang X, Wang J, Jiang H, Shi L, Xie J (2019) Hyperpolarization-activated cyclic nucleotide-gated channels: an emerging role in neurodegenerative diseases. *Front Mol Neurosci* 12:141. <https://doi.org/10.3389/fnmol.2019.00141>
  55. Grillner S, Hellgren J, Menard A, Saitoh K, Wikstrom MA (2005) Mechanisms for selection of basic motor programs—roles for the striatum and pallidum. *Trends Neurosci* 28(7):364–370. <https://doi.org/10.1016/j.tins.2005.05.004>
  56. Cui G, Jun SB, Jin X, Pham MD, Vogel SS, Lovinger DM, Costa RM (2013) Concurrent activation of striatal direct and indirect pathways during action initiation. *Nature* 494(7436):238–242. <https://doi.org/10.1038/nature11846>
  57. Liljeholm M, O'Doherty JP (2012) Contributions of the striatum to learning, motivation, and performance: an associative account. *Trends Cogn Sci* 16(9):467–475. <https://doi.org/10.1016/j.tics.2012.07.007>
  58. Cooper JA, Sagar HJ, Tidswell P, Jordan N (1994) Slowed central processing in simple and go/no-go reaction time tasks in Parkinson's disease. *Brain* 117(Pt 3):517–529. <https://doi.org/10.1093/brain/117.3.517>
  59. Bokura H, Yamaguchi S, Kobayashi S (2005) Event-related potentials for response inhibition in Parkinson's disease. *Neuropsychologia* 43(6):967–975. <https://doi.org/10.1016/j.neuropsychologia.2004.08.010>

**Publisher's Note** Springer Nature remains neutral with regard to jurisdictional claims in published maps and institutional affiliations.

Springer Nature or its licensor holds exclusive rights to this article under a publishing agreement with the author(s) or other rightsholder(s); author self-archiving of the accepted manuscript version of this article is solely governed by the terms of such publishing agreement and applicable law.